

# Computer graphics techniques for modeling page turning

Veronica Liesaputra · Ian H. Witten

Published online: 26 September 2009  
© Springer-Verlag 2009

**Abstract** Turning the page is a mechanical part of the cognitive act of reading that we do literally unthinkingly. Interest in realistic book models for digital libraries and other online documents is growing. Yet, actually producing a computer graphics implementation for modeling page turning is a challenging undertaking. There are many possible foundations: two-dimensional models that use reflection and rotation; geometrical models using cylinders or cones; mass-spring models that simulate the mechanical properties of paper at varying degrees of fidelity; and finite-element models that directly compute the actual forces within a piece of paper. Even the simplest methods are not trivial, and the more sophisticated ones involve detailed physical and mathematical models. The variety, intricacy, and complexity of possible ways of simulating this fundamental act of reading is virtually unknown. This article surveys computer graphics models for page turning. It combines a tutorial introduction that covers the range of possibilities and complexities with a mathematical synopsis of each model in sufficient detail to serve as a basis for implementation. Illustrations are included, which are generated through our implementations of each model. The techniques presented include geometric methods (both two- and three-dimensional), mass-spring models with varying degrees of accuracy and complexity, and finite-element models. We include a detailed comparison of experimentally determined computation time and subjective visual fidelity for all the methods discussed. The simpler techniques support convincing real-time implementations on ordinary workstations. We also address the question of whether such

techniques are worthwhile in practice by describing results from a user study that compared the performance of a page-turning book model with HTML and PDF presentations of the same material—and with physical books. This demonstrates that the book model has many advantages over conventional document formats.

**Keywords** Electronic book · User interface · 3D books

## List of symbols

$x, y, z$	Global coordinate system
$\xi, \eta, \zeta$	Local coordinate system
$\hat{x}, \hat{y}, \hat{z}$	Normal-vector coordinate system
$p$	Point in global coordinate
$p_i$	Reference point $i$ in global coordinate
$\pi$	Point in local coordinate
$\pi_i$	Reference point $i$ in local coordinate
$n$	Vector normal to the shell
$n_i$	Vector normal to the shell at reference point $i$
$d$	Displacement vector
$q_i$	Displacement vector for reference point $i$
$w_i(\xi, \eta)$	Interpolation function for reference point $i$
$t$	Element's thickness
$E$	Young's modulus
$\nu$	Poisson's ratio
$K$	Shear correction factor

V. Liesaputra (✉) · I. H. Witten  
Department of Computer Science, University of Waikato,  
Hamilton, New Zealand  
e-mail: vl6@cs.waikato.ac.nz

I. H. Witten  
e-mail: ihw@cs.waikato.ac.nz

## 1 Introduction

Digital libraries invariably present their documents in a manner that is rather bland. Much electronic text is formatted

for the screen in a way that is crude compared with typeset book pages. Some e-book designers do pay attention to look and feel, with crisp text, clearly formatted and attractively laid out [13]. Many digital library collections offer page images rather than electronic text, and although these can be rather beautiful, they are presented in a flat, two-dimensional manner.

In recent years, there has been an increased interest in modeling the act of turning a page. The British National Library's "Turning the pages" [4] is a pioneering project that aims to provide a reading experience closely resembling a real book. Readers view a screen showing a double-page spread of what looks similar to a physical rather than an electronic book. By wiping a finger across the touch-sensitive screen, they metaphorically pick up a page and turn it. Pages look three-dimensional; the book's binding moves slightly in sympathy as a page is turned; page edges to right and left indicate how far through the book you are.

In order to accomplish this, photographs have been taken at several intermediate points during each page turn—so that what is displayed is a stored photo, not an artifact computed from a model of the book. There are many images—for example, one version of the system consumes 300 Mb for only 20 book pages (this includes zoomed-in versions of each page, and accompanying audio). The system is constructed using Macromedia Director. The simulation is compelling, and users rapidly become absorbed in the book itself, turning pages unthinkingly. In Coleridge's words, they "willingly suspend disbelief" in these "shadows of imagination." However, the main drawback is that a slow animation of every page-turn must be painstakingly photographed in advance, for each book. This is not feasible as a delivery mechanism for online digital libraries.

Several more practical techniques for modeling the act of turning a page have been proposed [1–3, 6, 7, 19, 20] to handle overlapping windows. These include a simple two-dimensional effect that allows the lower left-hand corner to be moved and shows the paper as though it were creased flat, the position of the crease being adjusted to follow the motion; three-dimensional geometric techniques that wrap the paper around a cylinder or cone, physical simulations based on mass-spring models of the paper; and finite-element models that divide the paper into small elements and consider the physical constraints on each one, including its interactions with its neighbors. The aim of this article is to provide a detailed survey and explanation of all these methods.

Figure 1 shows the relationships between the various methods described in this article. There is a basic distinction between geometric and physical simulations. Ignoring the physical properties of paper, the former define appearance by a set of geometric equations, each of which relates to a particular user action. For example, one action represents turning the page from its lower corner, while another simulates the

paper being folded. Of course, there is an infinitude of possible user actions, and it is impossible to know them all in advance: in practice, one picks a limited set and restricts users accordingly. In this article, we only consider the case when a user picks the bottom corner of the page and turns it from the right to left side of the book; the algorithms are readily adjusted for the more general case where the user grasps the top left corner or (less usually) any point down the right-hand edge or even the top or bottom edge. We also assume that initially the page lies flat on the  $XY$  plane. We call this two-dimensional geometric model "peeling": it is described in Sect. 2. The standard graphics technique of "shearing" provides an alternative two-dimensional method of turning a rigid page, but it is very straightforward, and we do not describe it here (see, e.g. [22]). The basic idea of peeling can be easily extended to three dimensions, but at added computational cost. Section 3 describes two further three-dimensional geometric models, one based on a cylinder and the other on a cone.

Physical models are more realistic than geometric ones but considerably more demanding to compute. Figure 1 divides them into particle models and finite element models. The former use mass-spring models of the interactions between the particles comprising the paper and are described in Sect. 4. The masses and springs form a mesh, and the forces are summed over the mesh points and then integrated over time to obtain the velocity and acceleration of these points. The first model copes only with paper that has cloth-like flexibility; the second allows the paper to bend in more natural curves but still suffers from an unnatural twisting effect; while the third uses a more sophisticated model to rectify this twisting problem.

A more comprehensive physical modeling technique is the finite-element method, which calculates the force, velocity, and acceleration for each small element of the paper. This is described in Sect. 5. It is a rather complex operation, though for paper it is simpler than a full finite-element analysis because the material forms a thin shell that need not be split into elements in the  $Z$  direction (perpendicular to the paper surface).

Descriptions of these algorithms are scattered around the literature, and vary greatly in style and prerequisite knowledge. The aim of this article is to describe them all in a unified way, in sufficient detail to allow them to be understood, compared, debated, implemented, and tested. Section 6 discusses the methods and compares them in terms of computation time taken by an implementation of each one, and visual fidelity.

Once the page-turning act has been simulated, many more details must be attended to before arriving at a compelling model of a realistic book [9]. These include modeling the binding of the book, the motion of its covers, the interaction between the pages and the covers, and the effects of metadata such as usage and sectionalization. Although these details are

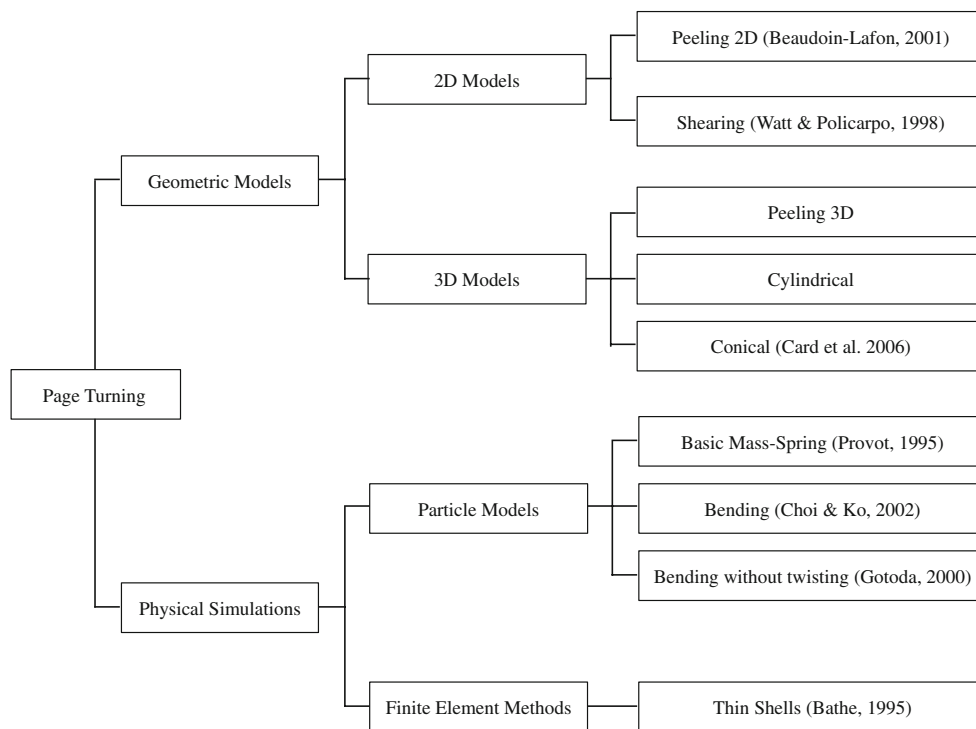


**Fig. 1** Page turning simulation

crucial to the implementation of a full and realistic physical book metaphor, they are not discussed in this article. It turns out that describing different techniques for page turning is a sufficiently ambitious goal.

We close by describing a user study that assesses the impact of reading electronic documents with realistic page-turning. We have built a lightweight implementation of a book model with the simplest page-turning technique (two-dimensional geometric model), which combines the operations we have come to expect from electronic formats, such as searching, animation, and multimedia, with the advantages of conventional books, such as page turning, easy and natural random-access navigation, bookmarks, annotation, and highlighting. Section 7 briefly describes this system and presents the results of an experimental comparison of its performance with conventional electronic formats (HTML and PDF) and with physical books. Each format is evaluated in terms of subjects' reading outcome measures, which include speed, reading comprehension and the participants' subjective opinions of the reading experience.

## 2 Two-dimensional geometric model

Imagine turning over the lower right-hand corner of a page and creasing it flat to reveal a triangular-shaped region of the page beneath—a “dog-ear”—with a corresponding triangular region that shows the text on the obverse side of the page.



**Fig. 2** Page turning using a two-dimensional geometric model

Imagine creating a sequence of successively larger dog-ears. This would be difficult physically (and would make a creased mess of the page), but is trivial in a computer model—and not messy at all. As the motion continues, the triangle grows and becomes a quadrilateral when it eventually subsumes the top right-hand corner of the page.

Figure 2 shows this peeling effect. Although the underlying model is entirely two-dimensional, visual details have been added to simulate the effect of a smooth bend rather than a sharp crease: some shading on the bend and some shadowing just beneath it. It is easy to perform the computation in real time as the page is turned. The method was proposed by Beaudouin-Lafon [2] to handle overlapping windows, and has been used in other page-turning projects [3, 19].

Although this simple model does not look terribly realistic in the static pictures of Fig. 2, it is surprisingly effective in practice. The readers define the path of the corner of the page as it turns: in effect they gesture with the mouse or touchscreen, and the corner of the page follows instantly—whether the motion is straight across to the left, or directly upward,

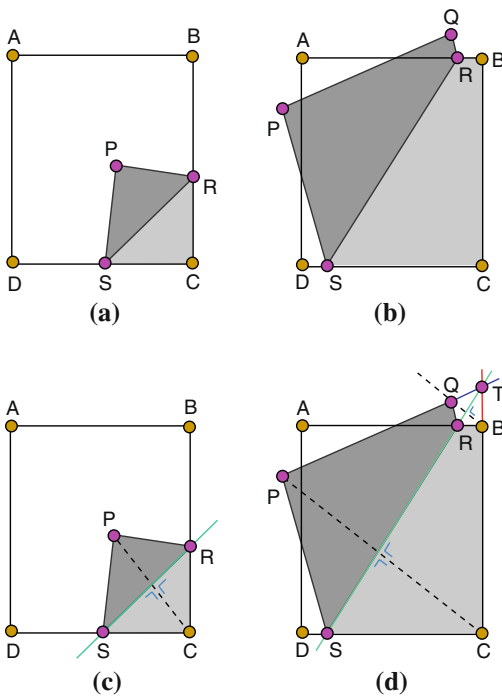


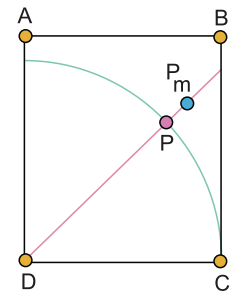
**Fig. 3** The appearance of the page: **a** when  $R$  intersects  $BC$ , **b** when  $R$  intersects  $AB$ . **c**, **d** shows the geometry of the page at situation (a) and (b), respectively

or even up and to the right. There is complete freedom to move the corner of the page (within the physical constraint imposed by not tearing the paper), and the crease and visual shading details follow instantly. The simulation is satisfyingly reactive.

This technique involves partitioning the page into three sections: the visible portion of the page being turned, part of the obverse side of the page that the turn has made visible, and the part of the following page that has been revealed. These regions are shaded differently in Fig. 3. The region formed by the crease (dark gray) can either be triangular, as in Fig. 3a, or quadrilateral, as in Fig. 3b. The area revealed (light gray) has exactly the same shape reflected in the axis formed by the crease. In these figures, the page’s initial position is the rectangle  $ABCD$ , and the act of turning has moved the lower right corner  $C$  to position  $P$ . The creased region is either the triangle  $PRS$  in Fig. 3a or the quadrilateral  $PQRS$  in Fig. 3b. The location of points  $Q$  (if applicable),  $R$  and  $S$ , are calculated from the position of point  $P$ .

Figure 3c,d show the geometry of the two situations. The crease is the perpendicular bisector of the line  $PC$ . The triangular configuration of Fig. 3c occurs when this bisector intersects the right-hand edge  $BC$  of the original page; the quadrilateral configuration of Fig. 3d occurs when it intersects the top edge  $AB$ . This allows the points,  $R$  and  $S$ , to be calculated. In Fig. 3d, we also need to calculate  $Q$ , which is obtained by drawing a line from corner  $B$  parallel to  $CP$ ,

**Fig. 4** Mapped position of the mouse



noting where it intersects the crease line (point  $M$ ), and producing it for an equal distance to locate point  $Q$ —effectively ensuring that the crease line is a perpendicular bisector of  $QB$  as well as of  $PC$ .

The paper imposes a physical constraint on where the page corner  $P$  can be, for the distance  $PS$  cannot exceed the length of  $CD$ . This constrains  $P$  to lie within the circle shown in Fig. 4; otherwise, the page would be torn from the spine. If the user moves the mouse outside the circle (say to position  $P_m$ ), it should be silently mapped to a point  $P$  on the arc of the circle. This feels perfectly natural because the system provides instant feedback by drawing the crease and filling in the contents of the region. Note that although we have described the technique using a portrait rather than a landscape layout, and turning from the lower right corner of the page instead of the upper right corner, it is straightforward to extend it to cover more general cases, including ones where the user picks up the page along an edge rather than at a corner.

The computational complexity of this technique is constant, independent of any grid size, and in practice, the system responds instantaneously to user actions. This method can be implemented entirely in Adobe Flash. Three images are maintained: the facing and reverse side of the page being turned, and the facing side of the page beneath. In order to show the creased region, the page’s obverse image is rotated to position its lower corner at  $P$  and upper corner at  $Q$  (if applicable), and a mask whose shape corresponds to the creased region is applied. In order to reveal the facing image of the page beneath, a mask shaped like the triangle  $RCS$  or quadrilateral  $RBCS$  is applied.

A shadow effect can be created using a transparent bitmap image that includes appropriate shading for the revealed part: it is rotated to place its centerline along  $SR$  and masked appropriately. Shading can be applied on both sides of the crease, not just to the page beneath. In addition, a small shadow can be applied to the top of the visible edge of the page being turned. These subtle effects, which can be seen by examining Fig. 2 closely, enhance the perception that the page is being turned in three dimensions. In addition, pages can easily be made slightly transparent so that readers see a hint of the page underneath.

A visual shortcoming of the peeling effect is that the creased area  $PRS$  is *exactly* the same as the revealed area

$CRS$  (or, in the quadrilateral case,  $PQRS$  is exactly the same as  $CBR S$ ). In a true three-dimensional page-turning situation, the extension of the paper in the  $Z$  direction will cause the turned area to be smaller than the revealed area. The three-dimensional bending of the page can be simulated by adding a  $Z$  value to each point  $P, Q, R,$  and  $S$ , and utilizing a spline function to make the bend look curvaceous instead of sharply creased. This makes the turned area smaller than the revealed area. The  $z$ -value of  $P$  can be assigned using a simple heuristic, and suitable values for  $Q, R,$  and  $S$  calculated from it. In practice, this necessitates segmenting the paper into a regular grid of size  $n \times m$  ( $n$  and  $m$  differ in proportion to the paper's aspect ratio). The use of a spline function raises the time complexity of the technique from constant to  $O(n^2)$ .

### 3 Three-dimensional geometric model

In two dimensions, the paper is creased and visual effects incorporated to make the crease look reasonably realistic. An alternative simulation of how the paper bends can be created in three dimensions by shaping the turned page as a cylinder or cone. There are many possible ways of doing this. One is to wrap the page around an imaginary cylinder or cone that rests on the  $XY$  plane, touching it along the  $Y$  axis (which corresponds to the spine of the book). The radius of the cylinder, or the angle of the cone, and the position of its apex on the negative  $Y$  axis, are varied to provide different degrees of curling.

As in the previous technique, the user controls the page turn by moving the point  $P$  that corresponds to its lower left-hand corner. In the cylinder model only the horizontal position ( $x$ -coordinate) of  $P$  can be controlled, and the page has exactly the same curvature all the way along the  $Y$  axis. In the conical model, both the  $x$  and  $y$  value of  $P$  can be controlled, and the position of the cone's apex is adjusted to fit. In both cases, the height ( $z$ -value) of  $P$  is calculated according to a simple heuristic. Of course, if a three-dimensional input device were available, then the user could control the height of  $P$ .

The first stage of the computation is to determine the parameters of the cylinder or cone from the position of  $P$ . In the second stage, the page is modeled as a uniform mesh of  $m \times n$  points, and as it is turned, it is necessary to calculate where each point maps to on the cylinder or cone.

#### 3.1 Cylindrical model

Imagine wrapping the paper around a cylinder of radius,  $r$ . At the beginning, the radius is effectively infinite, and the page lies flat on the  $XY$  plane. The cylinder axis is located along the  $Y$  axis. As the turn proceeds, the cylinder's radius is gradually reduced until the midpoint is reached. This causes

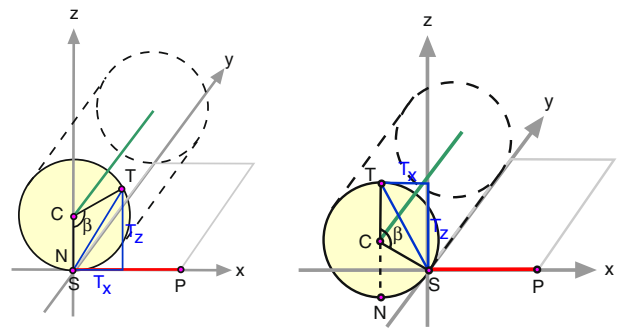


Fig. 5 Mapping a point to a cylinder

the page to curl around the cylinder, lifting its right-hand edge from the plane. From the midpoint onward, the radius gradually increases and the cylinder axis moves down and to the left, uncurling the page, until the radius becomes infinite when fully turned, and the page lies flat on the left-hand side of the book.

Let us assume that a user has moved the bottom right corner of the page  $P$  to position  $T$ . Based on the position of  $T$ , define a cylinder of radius  $r$  whose circular base passes point  $T$  and intersects the  $Y$  axis at point  $S$ , where the length of the arc  $ST$  equals the line  $SP$ , as shown in Fig. 5. If  $T$  has not passed the midpoint, then the angle between  $CN$  and  $CS$  is  $0$ . Otherwise, the angle between  $CN$  and  $CS$  is  $180^\circ - \beta$ . Point  $C$  is the center of the circle that lies on the cylinder's axis. The  $x$ -value of each mesh point is mapped to the cylinder, so  $O(n)$  operations are involved.

The result of this wrapping is rather stilted, and the page appears unnaturally rigid. The turning path parallels the  $X$  axis, which is not usually appropriate for single pages but can be useful when an entire multi-page section of a book is turned at once.

#### 3.2 Conical model

Readers seldom turn a page with a path that is parallel to the  $X$  axis. They generally lift the corner of the page and move it diagonally upward until it reaches the page midpoint, then diagonally downward from the midpoint onwards. Thus, only the grabbed corner should be lifted ahead of the mesh. In order to achieve this, Card et al. [6] use a conical model instead of a cylindrical one. The page-turning mechanism is similar to the cylindrical model except that it uses a cone instead of a cylinder. The shape of the cone is defined by its angle  $\theta$  and apex location  $A = (0, A_y, 0)$ . Different page trajectories can be obtained by varying these values.

Assume the reader has moved the bottom right corner of the page  $P$  to position  $T$ . Define a cone of radius  $r$  whose circular base passes through  $T$  and intersects the  $Y$  axis at the point  $S$  where the length of the arc  $ST$  equals the line  $SP$ , as shown in Fig. 6. As in the cylindrical model, if  $T$  has

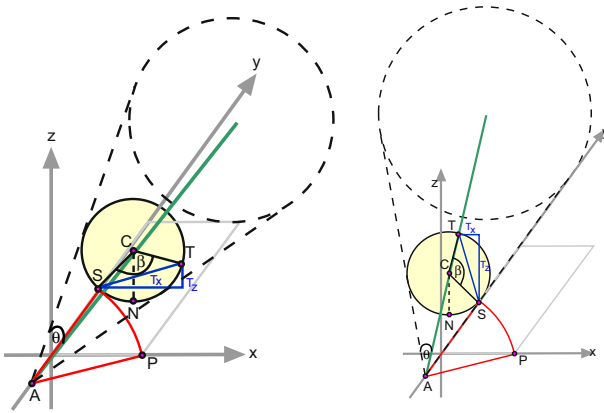


Fig. 6 Wrapping a page around a cone

not passed the midpoint, then the angle between  $CN$  and  $CS$  is 0; otherwise, it is  $180^\circ - \beta$ . Point  $C$  is the center of the circle that lies on the cone’s axis. Given the angle  $\beta$  between point  $T$ , the center of the cross section, and point  $S$ ,  $T$  can be obtained by first rotating  $S$  around the line  $X = 0, Z = r$  through an angle of  $\beta$  to the new position  $S' = (S'_x, S'_y, S'_z)$ , and then rotating it around the line  $Y = S_y, Z = 0$  through an angle of  $\theta$ . The radius  $r$  of the circle at each cross section varies, and so the deformed page is defined by mapping each mesh point onto the cone. The computational complexity of the algorithm is  $O(n^2)$ .

#### 4 Physical simulation using particle models

In particle models, the paper is simulated by dividing the material into a grid of small elements and modeling each element as though it were a single “particle.” The accuracy of the simulation is determined by the size of the grid: the result is more accurate with more elements, but needs more computation. Such models are often used in computer graphics to simulate cloth, such as flags waving in the breeze or folds of clothing draped upon a person’s body, and even hair. For page-turning, we divide the sheet of paper into  $m \times n$  small patches on a two-dimensional rectangular mesh. In reality, the patches flex, which is what gives paper its mechanical properties, but here we ignore this and treat each patch as though it were atomic.

In this model, the mechanical properties of the paper are simulated by a lattice of springs rather than the elasticity of the material itself. These springs, which are mass-less, model the interactions between the particles that comprise the paper. The force that the springs exert on each particle is calculated: this is called the “internal” force. “External” forces include the user’s page-turning action, constraints imposed by the book’s spine, and the force of gravity. Both types of force are summed, and the result is used to determine the defor-

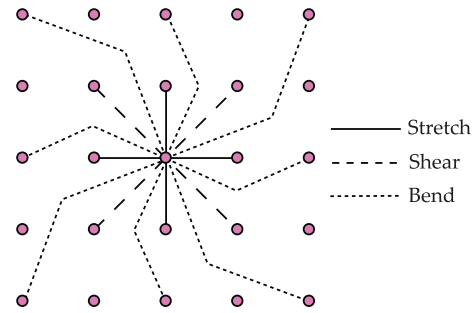


Fig. 7 Simple mass-spring model

mation of the paper at each given point in time. This kind of physical simulation has three major components: mesh representation; forces, both internal and external; and time integration.

Three different particle models are considered in this section. The first is for paper that flexes in a way that resembles cloth more than paper, the second allows more natural curved bends to develop, while the third incorporates a more sophisticated model of based on dihedral angles between constituent planes. In each case, we discuss the mesh representation, the forces applied and exerted, and how results are obtained by integrating the system of equations over time.

We denote by  $p_{ij}$  the particle at grid point  $i, j$ , where  $i = 1, 2, \dots, m$  and  $j = 1, 2, \dots, n$ . These positions depend on the current time  $h$ , but to simplify the notation, we do not show this dependence explicitly. The particle has a mass of  $m_{ij}$ . It is acted upon by the external forces of gravity and, depending on the particular values of  $i$  and  $j$ , by the user’s page-turning action and the spine constraints. The total external force is denoted by  $F_{\text{ext}}(p_{ij})$ :

$$F_{\text{ext}}(p_{ij}) = F_{\text{grav}}(p_{ij}) + F_{\text{user}}(p_{ij}) + F_{\text{spine}}(p_{ij}). \tag{1}$$

Two kinds of internal forces act on the particle: a damping force and the force exerted by all the springs attached to it. The internal force is designated by  $F_{\text{int}}(p_{ij})$ :

$$F_{\text{int}}(p_{ij}) = D(p_{ij}) + F_{\text{spring}}(p_{ij}). \tag{2}$$

The damping force  $D(p_{ij})$  is calculated from the damping constant and the node’s velocity, while the spring force  $F_{\text{spring}}(p_{ij})$  is computed from the displacements of the node and those nodes to which it is attached, and each spring’s stiffness constant.

The sum of the external and internal forces on the particle is

$$F_{ij} = F_{\text{ext}}(p_{ij}) + F_{\text{int}}(p_{ij}). \tag{3}$$

The value of this at time  $h$  is used to determine the particle’s position at time  $h + \Delta h$ . We do this operation on each particle in the grid, so  $O(n^2)$  operations are involved.

### 4.1 Basic particle model

In the simplest type of particle model, developed by Provot [20], nodes are connected with three types of mass-less springs as shown in Fig. 7: stretch, shear, and bend springs.

1. Stretch springs connect  $\mathbf{p}_{ij}$  with  $\mathbf{p}_{i\pm 1,j}$  and  $\mathbf{p}_{i,j\pm 1}$ .
2. Shear springs connect  $\mathbf{p}_{ij}$  with  $\mathbf{p}_{i\pm 1,j\pm 1}$ .
3. Bend springs connect  $\mathbf{p}_{ij}$  with  $\mathbf{p}_{i\pm 2,j}$ ,  $\mathbf{p}_{i,j\pm 2}$  and  $\mathbf{p}_{i\pm 2,j\pm 2}$ .

Springs produce a force that depends on their length and stiffness constant. The stiffness is the same for all springs of a given type.

These springs are responsible for simulating the paper’s stretch, shear, and bend resistance. Stretch springs define the resistance of the material to elongation or compression in the horizontal and vertical directions. Shear springs define the resistance in diagonal directions. When the paper is bent, particle  $\mathbf{p}_{ij}$  moves closer to its next-nearest-neighbor particles, and the paper’s bend resistance is calculated from the distance of  $\mathbf{p}_{ij}$  to its eight next-nearest-neighbors.

#### 4.1.1 Effect of forces

We denote the stiffness constant of the spring linking particles  $\mathbf{p}_{ij}$  and  $\mathbf{p}_{kl}$  by  $K_{ij,kl}$ , and the rest length of the spring, which is its initial length at time  $h = 0$ , by  $l_{ij,kl}^0$ . The length of the spring at time  $h$  is  $l_{ij,kl} = |\mathbf{p}_{kl} - \mathbf{p}_{ij}|$ . According to Hooke’s Law, the total spring force on  $\mathbf{p}_{ij}$  is given by

$$\mathbf{F}_{\text{spring}}(\mathbf{p}_{ij}) = \sum_{(k,l) \in R} -K_{ij,kl} (|l_{ij,kl}| - |l_{ij,kl}^0|) \frac{l_{ij,kl}}{|l_{ij,kl}|} \quad (4)$$

where the sum is over  $R$ , the set of nodes that are connected with  $\mathbf{p}_{ij}$ .

The damping force for node  $\mathbf{p}_{ij}$  is

$$\mathbf{D}(\mathbf{p}_{ij}) = -K_d \dot{\mathbf{p}}_{ij}, \quad (5)$$

where  $K_d$  is the damping coefficient of the paper and  $\dot{\mathbf{p}}_{ij}$  is the velocity of  $\mathbf{p}_{ij}$ .

#### 4.1.2 Limit strain

The elasticity of real materials is nonlinear. Once a certain degree of elongation has been reached, they become very stiff extremely rapidly when stretched further. If the applied load is high, then the material will rupture; however, we will not attempt to model ruptures. Figure 8a shows the appearance of a piece of paper that has been stretched unreasonably, a problem that we will proceed to fix.

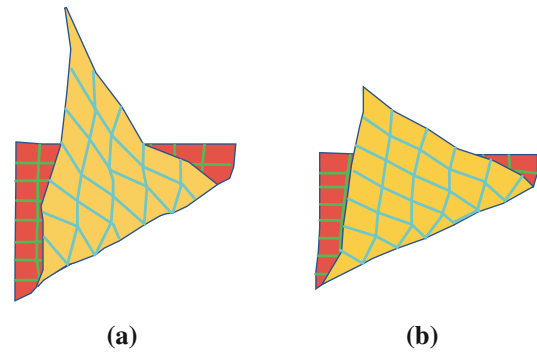


**Fig. 8** The appearance of the page: **a** without limit straining, **b** with limit straining

We define the amount of elongation as

$$\tau = \frac{|l_{ij,kl}| - |l_{ij,kl}^0|}{|l_{ij,kl}^0|} \quad (6)$$

and limit it to a predetermined constant  $\tau_c$  (normally set to 10%). If the elongation threatens to exceed  $\tau_c$  the nodes are brought closer together to bring it back to this value. This is done by moving the both particles towards their mid-point if they are both loose, while if one is fixed—e.g., if it lies on to the book’s spine—then the other is moved closer to it. The result is shown in Fig. 8b, where each spring has been limited to a predefined maximum elongation.

#### 4.1.3 Integrating over time

Given each node’s position  $\mathbf{p}_{ij}$ , velocity  $\dot{\mathbf{p}}_{ij}$  and total force  $\mathbf{F}_{ij}$  at time  $h$ , our goal is to determine the position  $\mathbf{p}'_{ij}$  and velocity  $\dot{\mathbf{p}}'_{ij}$  at time  $h + \Delta h$ . According to Newton’s law, the acceleration at time  $h + \Delta h$  is

$$\ddot{\mathbf{p}}'_{ij} = \frac{\mathbf{F}_{ij}}{m_{ij}}. \quad (7)$$

Using explicit Euler time integration,

$$\begin{aligned} \dot{\mathbf{p}}'_{ij} &= \dot{\mathbf{p}}_{ij} + \ddot{\mathbf{p}}'_{ij} \Delta h \\ \mathbf{p}'_{ij} &= \mathbf{p}_{ij} + \dot{\mathbf{p}}'_{ij} \Delta h. \end{aligned} \quad (8)$$

These equations are used to update the nodes’ position and velocity at every time step.

### 4.2 Bending

We now describe a more advanced mass-spring model developed by Choi and Ko [7] that can be bent into smooth curves. Paper is strongly resistant to stretching or shearing, but has little initial resistance to compression. However, when a certain degree of compression has been reached, it rapidly becomes stiffer under further compression. In order to simulate this,

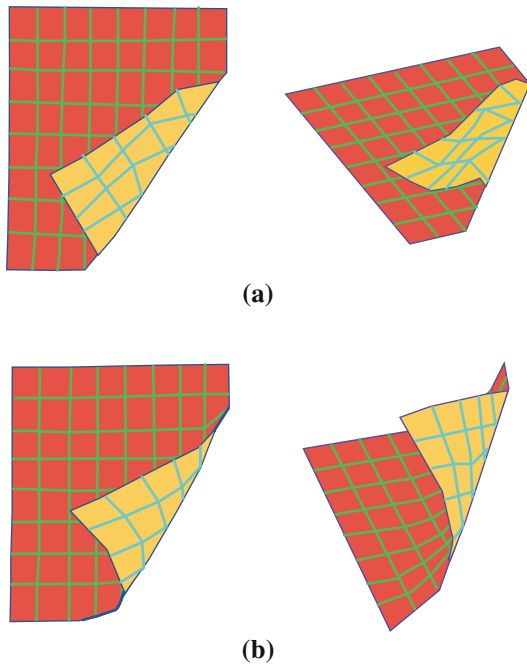


**Fig. 9** The appearance of the page: **a** using the simple mass-spring model of Sect. 4.1, **b** using the improved model of Sect. 4.2

a more sophisticated damping, bending, and compression model is needed.

Figure 9a shows how unnatural bending can look with the previous model. The page behaves in a manner more akin to cloth than paper, with insufficient resistance to the bending force—it crumples rather than bending stiffly and smoothly as paper does. In contrast, Fig. 9b shows a smoothly contoured bend that is produced by the model we develop in this section.

While it would be perfectly possible to use the same explicit time integration that was developed in the previous section for this new model, it would be much slower. In order to make the system respond quickly to the user’s interaction, semi-implicit time integration is used, instead. This is more stable than the explicit integration procedure, so large time steps can be used to reach the equilibrium state quickly.

Each particle is connected with others in the mesh in the same manner as before, and again all the springs of the same type have the same stiffness constant. However, different formulae are used to calculate the spring forces. Stretch and shear springs only affect the paper’s resistance to elongation in the vertical, horizontal, and diagonal directions, while bend springs affect its resistance to bending and compression in these directions.

4.2.1 Effect of forces

Let  $K_{ij,kl}$  denote the stiffness constant of a spring connecting  $\mathbf{p}_{ij}$  to  $\mathbf{p}_{kl}$ , and  $l_{ij,kl}^0$  the spring’s initial length at time  $h = 0$ . The length of the spring at time  $h$  is  $l_{ij,kl} = \|\mathbf{p}_{kl} - \mathbf{p}_{ij}\|$ . The

total spring force on  $\mathbf{p}_{ij}$  is given by

$$\mathbf{F}_{\text{spring}}(\mathbf{p}_{ij}) = \sum_{(k,l) \in R_s} \mathbf{s}_{ij,kl} + \sum_{(k,l) \in R_b} \mathbf{b}_{ij,kl} \tag{9}$$

where the sums are over  $R_s$ , the set of nodes connected to  $\mathbf{p}_{ij}$  by stretch and shear springs, and  $R_b$ , the set of particles connected to  $\mathbf{p}_{ij}$  by bend springs.

The force exerted by the stretch and shear springs is the same as before (Eq. 4) for elongation but zero for compression:

$$\mathbf{s}_{ij,kl} = \begin{cases} -K_{ij,kl} \left( \|l_{ij,kl}\| - l_{ij,kl}^0 \right) \frac{l_{ij,kl}}{\|l_{ij,kl}\|} & : \|l_{ij,kl}\| \geq l_{ij,kl}^0 \\ 0 & : \|l_{ij,kl}\| < l_{ij,kl}^0 \end{cases} \tag{10}$$

The force exerted by the bend springs is

$$\mathbf{b}_{ij,kl} = \begin{cases} 0 & : \|l_{ij,kl}\| \geq l_{ij,kl}^0 \\ -K_{ij,kl} f_b \left( \frac{\|l_{ij,kl}\|}{l_{ij,kl}^0} \right) \frac{l_{ij,kl}}{\|l_{ij,kl}\|} & : \|l_{ij,kl}\| < l_{ij,kl}^0 \end{cases} \tag{11}$$

This equation models the nonlinear nature of bend resistance. The shape of buckled paper is close to a circular arc. We approximate the arc’s length by the spring’s rest length  $l_{ij,kl}^0$  and express the curvature as a function of the distance between the particles. Choi and Ko [7] approximated the curvature function  $f_b$  as a fourth-order polynomial,

$$f_b(s) = -a_4s^4 + a_3s^3 - a_2s^2 + a_1s - a_0$$

where positive numeric values for the coefficients  $a_4, a_3, a_2, a_1$  and  $a_0$  were derived from the physical deformation constants that characterize the material in question.

In the previous model we used the same damping constant for stretch, shear and bend (Eq. 5). However, paper resists stretching and shearing much more than it resists bending, and this requires higher values for the these two damping constants than for the bend damping constant. This was not done in the previous model because bending looked unrealistic anyway. Now we would like to reduce the bend damping constant—but this causes unrealistic in-plane oscillations. In order to inhibit these requires a more sophisticated damping model than the one developed in the previous section. If  $K_d ij, kl$  is the damping constant of the spring linking particles  $\mathbf{p}_{ij}$  and  $\mathbf{p}_{kl}$ , the total damping force on  $\mathbf{p}_{ij}$  is

$$\mathbf{D}(\mathbf{p}_{ij}) = - \sum_{(k,l) \in R} K_d (\dot{\mathbf{p}}_{ij} - \dot{\mathbf{p}}_{kl}) \tag{12}$$

where  $R$  is the list of nodes that are connected to  $\mathbf{p}_{ij}$  by any type of spring.

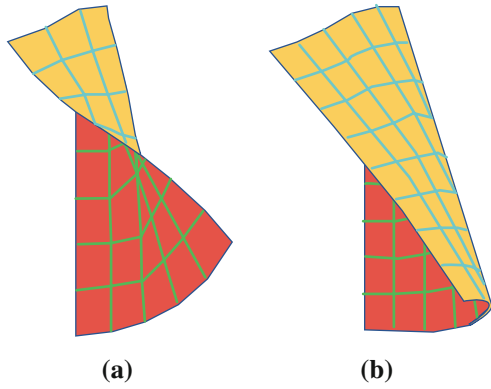


**Fig. 10** The appearance of the page: **a** using model of Sect. 4.2, **b** using improved bending model of Sect. 4.3

4.2.2 Integrating over time

In this model, semi-implicit time integration with a second-order backward difference formula is used to calculate the new position of particle  $\mathbf{p}_{ij}$  with mass  $m_{ij}$ . Let  $\mathbf{P}_{ij}$  and  $\dot{\mathbf{p}}_{ij}$  be the position and velocity at time  $h - \Delta h$ , and  $\mathbf{p}'_{ij}$  and  $\dot{\mathbf{p}}'_{ij}$  the position and velocity at time  $h$ . Given this information, the new position  $\mathbf{p}''_{ij}$  and velocity  $\dot{\mathbf{p}}''_{ij}$  at time  $h + \Delta h$  can be calculated as follows:

$$\begin{aligned} \Delta \mathbf{p}''_{ij} &= \frac{1}{\Delta h} \left( \frac{3}{2} \mathbf{p}'_{ij} - 2\mathbf{p}_{ij} + \frac{1}{2} \mathbf{P}_{ij} \right) \\ \Delta \dot{\mathbf{p}}''_{ij} &= \frac{1}{\Delta h} \left( \frac{3}{2} \dot{\mathbf{p}}'_{ij} - 2\dot{\mathbf{p}}_{ij} + \frac{1}{2} \dot{\mathbf{P}}_{ij} \right) \end{aligned} \tag{13}$$

These quantities must also satisfy the equation

$$\begin{pmatrix} \Delta \mathbf{p}''_{ij} \\ \Delta \dot{\mathbf{p}}''_{ij} \end{pmatrix} = \begin{pmatrix} \dot{\mathbf{p}}''_{ij} \\ \frac{\mathbf{F}''_{ij}}{m_{ij}} \end{pmatrix} \tag{14}$$

and

$$\mathbf{F}''_{ij} = \mathbf{F}'_{ij} + \sum_{(k,l) \in R} \left( \frac{\partial \mathbf{F}''_{ij}}{\partial \mathbf{p}''_{kl}} \Delta \mathbf{p}''_{kl} + \frac{\partial \mathbf{F}''_{ij}}{\partial \dot{\mathbf{p}}''_{kl}} \Delta \dot{\mathbf{p}}''_{kl} \right). \tag{15}$$

where  $R$  is the list of nodes that are connected to  $\mathbf{p}_{ij}$  by any type of spring.

4.3 Bending without twisting

Previous sections modeled the resistance of the paper to bending using springs that connect each particle with its next-nearest-neighbors. This model is simplistic because these springs are insensitive changes in the dihedral angles between faces. We now take this into account by changing the way the bending force is calculated.

The effect can be seen in Fig. 10, which shows a page using the model in the previous section and the model that will be developed in this section. Clearly, the latter looks

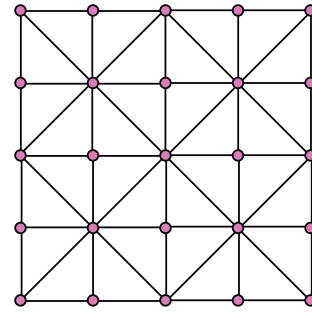


**Fig. 11** Mesh representation

more realistic, because the twist in the edge nearest to the viewer has been eliminated.

In this model, the paper is discretized into a set of right-angled triangles, as shown in Fig. 11. Initially, the paper is flat, and  $z = 0$  for each particle. In order to calculate the internal forces on the triangles instead of on each particle, slightly different formulae are used to determine the material’s resistance to stretching, shearing, and bending.

4.3.1 Effect of forces

The improved bending model is better expressed in terms of energies rather than forces as we did above; we can calculate the forces as the spatial derivative of energy. As before, three types of energy—stretch, shear, and bend—are used to characterize the difference between the undeformed configuration and the deformed one. The internal energy working on each particle  $\mathbf{p}_{ij}$  is

$$E_{\text{spring}} = \sum_{x \in T} E_{\text{stretch}}(x) + \sum_{x \in L} E_{\text{shear}}(x) + \sum_{x \in B} E_{\text{bend}}(x)$$

where  $T$  is the set of all triangles containing particle  $\mathbf{p}_{ij}$ ,  $L$  is the set of all edges that are connected to particle  $\mathbf{p}_{ij}$ , and  $B$  is the set of all edges that are connected to particle  $\mathbf{p}_{ij}$  and shared by two triangles. The stretch component relates to the triangle’s area, the shear component to the length of its edges, and the bend component to the dihedral angle with adjacent triangles; these three components are discussed further below. The total internal force at particle  $\mathbf{p}_{ij}$  is obtained by differentiating the energy:

$$\mathbf{F}_{\text{spring}}(\mathbf{p}_{ij}) = \frac{\partial E_{\text{spring}}}{\partial \mathbf{p}_{ij}}.$$

Stretch energy is produced by the triangle’s resistance to stretching or compression, which corresponds to changes in the triangle’s area. Let  $A^0$  be its initial area ( $h = 0$ ) and  $A^h$  be its area at time  $h$ . The stretch energy for the triangle is

$$E_{\text{stretch}}(x) = -K_{\text{stretch}} A^0 \left( 1 - \frac{A^h}{A^0} \right)^2, \tag{16}$$

where  $K_{\text{stretch}}$  is the stretch stiffness constant.

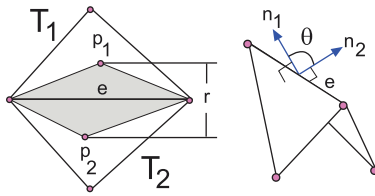


**Fig. 12** Components to calculate the mean curvature

Shear energy is produced by the triangle's resistance to shearing, which corresponds to changing the length of its edges but not its area. The shear energy for the triangle is the sum of the shear energies for each of its edges. Consider the edge  $e$ . Let  $l^0$  be its initial length (at time  $h = 0$ ) and  $l^h$  its length at time  $h$ . The shear energy that works on the edge is

$$E_{\text{shear}}(x) = -K_{\text{shear}} |l^0| \left( 1 - \frac{|l^h|}{|l^0|} \right)^2 \quad (17)$$

where  $K_{\text{shear}}$  is the shear stiffness constant.

Bending energy is produced by altering the mean curvature between two triangles that share the same edge. The bending energy for the triangle is the sum of the bending energies for each edge that borders a neighboring triangle. Figure 12 shows two triangles  $T_1$  and  $T_2$  that share a common edge  $e$ . Their initial (flat) position is shown unshaded; the shaded triangles are leaning upward, toward the viewer. The angle between the triangles at time  $h$  is

$$\theta^h = \tan^{-1} \left( \frac{\sin \theta^h}{\cos \theta^h} \right) \quad (18)$$

The sine and cosine can be expressed in terms of  $\mathbf{n}_1^h$  and  $\mathbf{n}_2^h$ , the unit normal vectors to  $T_1$  and  $T_2$  at time  $h$ , and the length  $l^h$  of the edge  $e$  at time  $h$ :

$$\begin{aligned} \sin \theta^h &= \left( \mathbf{n}_1^h \times \mathbf{n}_2^h \right) \cdot \frac{l^h}{|l^h|} \\ \cos \theta^h &= \mathbf{n}_1^h \cdot \mathbf{n}_2^h \end{aligned}$$

Denote the heights of triangles  $T_1$  and  $T_2$ , measured from the shared edge  $e$  to the opposite vertex, by  $t_1$  and  $t_2$ . The initial curvature span is the distance between the two triangles' centers of gravity in the initial position, which is  $r = \frac{1}{6}(t_1 + t_2)$ . The bending energy of edge  $e$  is

$$E_{\text{bend}} = -K_{\text{bend}} \frac{|l^0|}{r} (\theta^h - \theta^0)^2 \quad (19)$$

We use the same formulae as before, Eq. 12 above, to calculate the damping force exerted on particle  $p_{ij}$  through its interaction with particle  $p_{kl}$ .

#### 4.3.2 Integrating over time

Newmark implicit time integration is used for this model. This method gives the new position and velocity of particle  $p_{ij}$  at time  $h + \Delta h$  as

$$\begin{aligned} \mathbf{p}'_{ij} &= \mathbf{p}_{ij} + \Delta h \dot{\mathbf{p}}_{ij} + \frac{\Delta h^2}{4} \left( \ddot{\mathbf{p}}_{ij} + \ddot{\mathbf{p}}'_{ij} \right) \\ \ddot{\mathbf{p}}'_{ij} &= \ddot{\mathbf{p}}_{ij} + \frac{\Delta h}{2} \left( \ddot{\mathbf{p}}_{ij} + \ddot{\mathbf{p}}'_{ij} \right) \end{aligned}$$

The acceleration at time  $h + \Delta h$  is given by

$$\ddot{\mathbf{p}}'_{ij} = \frac{\mathbf{F}_{ij}}{m_{ij}} \quad (20)$$

where  $m_{ij}$  is  $p_{ij}$ 's mass.

## 5 Physical simulation using the finite element method

The finite element method is a general technique for simulating any physical material. The material is divided into a regular grid of small elements in three-dimensional space whose size determines the accuracy of the simulation. Such models are used to help design and develop products in many fields of engineering, particularly for investigating tradeoffs between maximizing stiffness and strength and minimizing weight, materials, and cost. For example, one might investigate how a car deforms under stress such as crash. In such situations, the finite element method allows entire designs to be constructed, refined, and optimized before any manufacturing takes place.

In the special case of page turning, we can take advantage of the quasi-two-dimensional nature of paper by using a two-dimensional rectangular mesh rather than a full three-dimensional grid, dividing a sheet of paper into  $m \times n$  small patches (Fig. 13). However, in the finite-element method, patches are not modeled as particles as they were in the previous section: instead, their dimensions and shape are taken into account. The forces on a patch—including gravity, forces exerted by neighboring patches, and the force the reader applies to turn the page—produce the stress which deforms the patch, and the finite element method calculates the amount of deformation. Note that although the grid is two-dimensional, the thickness of the paper is not ignored: each patch does have thickness, which varies across the patch.

Modeling paper as a thin shell, represented by a two-dimensional rectangular mesh of patches whose thickness varies, is a special case of the general finite element model of a three-dimensional solid, and is slightly easier to tackle than the general case. The first task is to establish a geometric mapping between the patches themselves and the global coordinate system (Sect. 5.1). Ultimately, we need to consider the physical forces on each patch—the stress—and work out the

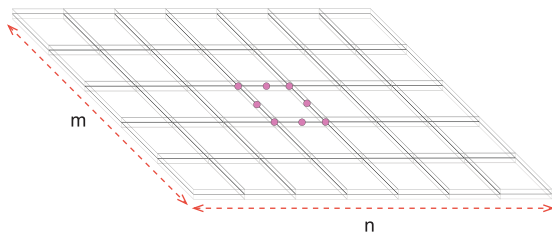


Fig. 13 Dividing a sheet of paper into  $m \times n$  elements

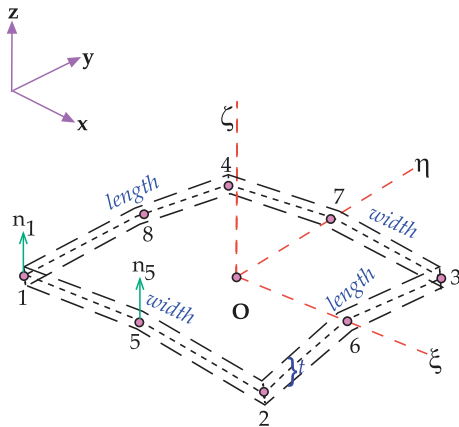


Fig. 14 An element of the shell

distortion they cause—the strain. Strain is defined in terms of the spatial derivatives of a point’s displacement, and calculating the stress–strain relationship involves differential equations. This requires a smooth, differentiable model of the patch; obtaining this is the second task (Sect. 5.2). It is necessary to model the patches not just as two-dimensional surfaces but as having thickness; the third task (Sect. 5.3). Then, we need to establish a three-dimensional coordinate system at each reference point of the patches (Sect. 5.4), and express the displacement of the reference points in terms of these coordinates (Sect. 5.5).

In terms of local coordinates the relationship between stress (Sect. 5.6) and strain (Sect. 5.7) is simple: it is given by a deformation matrix (Sect. 5.8) whose components depend on the Young’s modulus, Poisson’s ratio, and shear correction factor of the material under consideration, and it is easy to obtain reasonable estimates of these for paper. The relationship, which involves first derivatives of displacement, must be mapped back into global coordinates in order for it to be solved. We need to consider all the forces on each element, and finally integrate the differential equations that have been obtained (Sect. 5.9).

### 5.1 Local and global coordinates

Figure 14 shows a general element [5]. It is defined by eight reference points, four representing its corners and four representing the mid-points of each side. In global  $(x, y, z)$

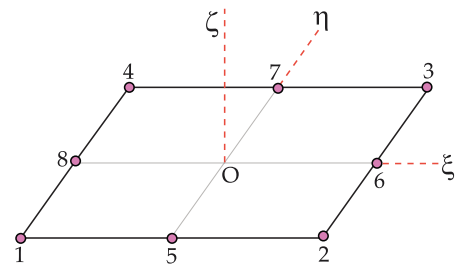


Fig. 15 Midsurface of the shell in local coordinate

Table 1 Local coordinates of the eight reference points

$i$	$(\xi_i, \eta_i, \zeta_i)$
1	$(-1, -1, 0)$
2	$(1, -1, 0)$
3	$(1, 1, 0)$
4	$(-1, 1, 0)$
5	$(0, -1, 0)$
6	$(1, 0, 0)$
7	$(0, 1, 0)$
8	$(-1, 0, 0)$

coordinates these reference points are  $p_1, p_2, p_3$  and  $p_4$  for the first group and  $p_5, p_6, p_7$  and  $p_8$  for the second: each  $p_i$  has coordinates  $(x_i, y_i, z_i)$  in ordinary three-dimensional space. If thickness is modeled, the reference points are taken to be at the center of the material and further parameters  $t_1 \dots t_8$  give the corresponding thicknesses, so that at each reference point the material of the paper extends from  $-\frac{t_i}{2}$  to  $+\frac{t_i}{2}$ . The direction of this extension is normal to the paper at point  $p_i$ , a direction that we call  $n_i$ .

Figure 15 shows the local coordinate system that is defined for each patch. Any point within the element is given by coordinates,  $(\xi, \eta, \zeta)$ , where all the coordinates lie between  $-1$  and  $+1$ .  $\xi$  and  $\eta$  give the extent in directions corresponding to the width and height of the paper, respectively; while  $\zeta$  is the direction perpendicular to the paper, and corresponds to its thickness. Reference point  $p_1$ , which lies in the center of the paper, has local coordinates  $\pi_1 = (-1, -1, 0)$ , while point  $p_3$  has local coordinates  $\pi_3 = (1, 1, 0)$ . The upper surface of the paper at  $p_3$  is  $(1, 1, 1)$ , while the lower surface is  $(1, 1, -1)$ . We use the symbol  $\pi$  to denote the local  $(\xi, \eta, \zeta)$  coordinates of the point whose global  $(x, y, z)$  coordinates are  $p$ , for the element in question. Table 1 shows the local coordinates of the eight reference points.

Each patch is fully defined by the position in space of its eight reference points, and the coherence of the assembly of patches is ensured by making the three points that define one side of a patch correspond to the three points that define the adjacent side of the neighboring patch in the obvious manner, all the way along both the height and the width of the paper.

5.2 Defining a smooth surface

We next address the problem of how to define from this grid of reference points, a smooth and continuous surface for each patch. In fact, it is not necessary to fit a smooth surface to present the patch on the computer screen: for that purpose the discrete grid of reference points is entirely adequate. Rather, a smooth surface is needed because the analysis in subsequent subsections in terms of stress and strain involves spatial derivatives of the surface.

We restrict our attention to a particular patch. Given a point on the midsurface of this patch whose local coordinates are  $\boldsymbol{\pi} = (\xi, \eta, 0)$  ( $\zeta = 0$  because it is on the midsurface), what is its global coordinate vector  $\boldsymbol{p} = (x, y, z)$ ? The vector  $\boldsymbol{p}$  will be expressed as a weighted sum of the vectors  $\boldsymbol{p}_1, \boldsymbol{p}_2, \dots, \boldsymbol{p}_8$  that represent the eight reference points of the patch, where the weights  $w_1(\xi, \eta), w_2(\xi, \eta), \dots, w_8(\xi, \eta)$  reflect the position of the point  $\boldsymbol{\pi}$  in local coordinate space:

$$\boldsymbol{p} = \sum_{i=1}^8 w_i(\xi, \eta) \boldsymbol{p}_i \tag{21}$$

For example, if  $\boldsymbol{\pi}$  corresponds with one of the reference points, the weights will be 1 for that reference point and 0 for the other seven points.

If the patch were planar, then this would be a simple matter of linear interpolation. However, in general, the points  $\boldsymbol{p}_1, \boldsymbol{p}_2, \dots, \boldsymbol{p}_8$  do not lie on a plane in 3-space. In order to account for this, it is necessary to define eight nonlinear interpolation functions  $w_i(\xi, \eta)$  with the following properties:

1.  $\sum_{i=1}^8 w_i(\xi, \eta) = 1$  for any values  $\xi, \eta \in [-1, 1]$
2.  $w_i(\xi_i, \eta_i) = 1$  for each reference point,  $i = 1, 2, \dots, 8$
3.  $w_i(\xi_j, \eta_j) = 0$ , if  $j \neq i$ .

It turns out that while linear interpolation is inadequate to model a nonplanar patch, quadratic weighting functions can be constructed, which satisfy these properties. Figure 16a shows a suitable function  $w_1(\xi, \eta)$  for reference point 1 of the patch: as can be seen, it satisfies properties 2 and 3 with  $i = 1$ . We construct this function by taking the component shown in Fig. 16b and subtracting the components in Fig. 16c,d. Figure 16b is a bilinear surface that satisfies property 2 at reference point 1, and satisfies property 3 at points 2, 3, 4, 6, and 7 but violates it at points 5 and 8; Fig. 16c is a parabolic correction that restores property 3 at point 5; and Fig. 16d does the same for point 8.

The bilinear function in Fig. 16b has equation

$$\frac{1}{4}(1 - \xi)(1 - \eta).$$

This alters the function's value for reference point  $\boldsymbol{\pi}_1 = (-1, -1, 0)$  as desired, and evaluates to 0 at any reference points with either  $\xi = 1$  or  $\eta = 1$ —that is, points  $\boldsymbol{\pi}_2, \boldsymbol{\pi}_6, \boldsymbol{\pi}_3,$

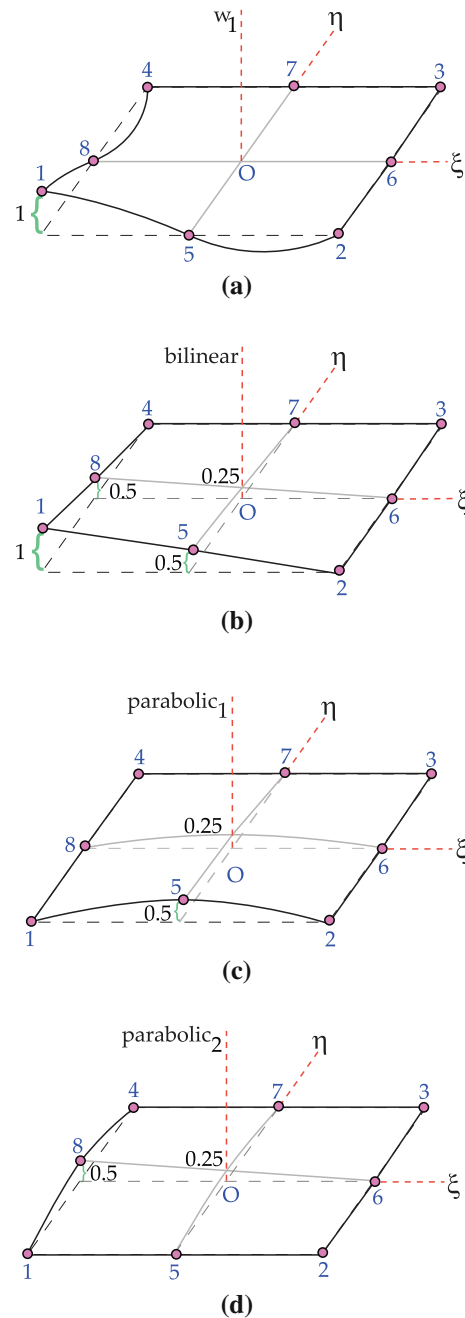


**Fig. 16** Creating **a** the interpolation function  $w_1$  by adding three functions: **b** bilinear, **c** parabolic<sub>1</sub>, **d** parabolic<sub>2</sub>

$\boldsymbol{\pi}_7, \boldsymbol{\pi}_4$ . It also has the undesired effect of evaluating to 0.5 at points  $\boldsymbol{\pi}_5$  and  $\boldsymbol{\pi}_8$ , as shown. The parabolic functions in Fig. 16c,d have equations

$$\frac{1}{4}(1 - \xi^2)(1 - \eta) \quad \text{and} \quad \frac{1}{4}(1 - \xi)(1 - \eta^2).$$

These both evaluate to 0 at points  $\boldsymbol{\pi}_1, \boldsymbol{\pi}_2, \boldsymbol{\pi}_6, \boldsymbol{\pi}_3, \boldsymbol{\pi}_7$  and  $\boldsymbol{\pi}_4$ , and 0.5 at  $\boldsymbol{\pi}_5$  and  $\boldsymbol{\pi}_8$ , respectively. Thus the overall effect of raising to 1 the weighting function's value at reference point  $\boldsymbol{\pi}_1$ , shown in Fig. 16a, is accomplished by

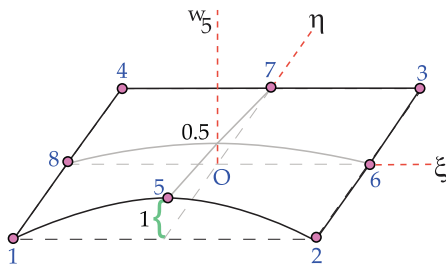


Fig. 17 Interpolation function  $w_5$

$$w_1(\xi, \eta) = \text{bilinear} - \text{parabolic}_1 - \text{parabolic}_2$$

$$= \frac{1}{4}(1 - \xi)(1 - \eta)(-1 - \xi - \eta)$$

The weighting functions for the other three corners  $\pi_2, \pi_3,$  and  $\pi_4$  are accomplished in similar manner.

The weighting function for the mid-point of a side is simpler, requiring only a single parabolic model as shown in Fig. 17 for  $\pi_5$ .

In summary, we have established weighting functions that have the value of 1 at a reference point and 0 at the other seven reference points. These functions are

$$w_i(\xi, \eta) = \begin{cases} \frac{1}{4}(1 + \xi\xi_i)(1 + \eta\eta_i)(-1 + \xi\xi_i + \eta\eta_i) & i \in [1, 4] \\ \frac{1}{2}(1 - \xi^2)(1 + \eta\eta_i) & i \in \{5, 7\} \\ \frac{1}{2}(1 + \xi\xi_i)(1 - \eta^2) & i \in \{6, 8\} \end{cases} \quad (22)$$

Not only do they satisfy properties 2 and 3 above, but it can be shown algebraically that the eight functions sum to 1 for any values of  $\xi, \eta$ , thus satisfying property 1, too. Furthermore, the values of all the eight interpolation functions along any edge are defined purely by the three reference points that constitute that edge; thus  $(x, y, z)$  coordinates of any point along an edge will be the same as for the neighboring patch, making the entire surface continuous. However, the first derivative across an edge is *not* continuous, which means that creases in the paper such as dogeared pages—or even a crumpled ball of paper—can be modeled.

### 5.3 Inside the shell

The discussion so far has focused on points on the midsurface of the shell. We will also need to deal with general points inside the shell,  $\pi = (\xi, \eta, \zeta)$  with  $\zeta \neq 0$ . For this, we need to establish vectors normal to the shell at each of the reference points, as shown in Fig. 18.

In the beginning, each element of the shell is represented by the coordinates of the top and bottom surfaces at each of the eight reference positions, rather than the reference points themselves. Then, at each reference position, the actual

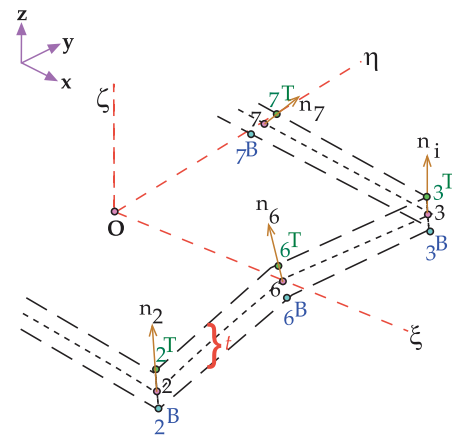


Fig. 18 Normal vector of the shell's midsurface

reference point is calculated by averaging the coordinates of the top and bottom surfaces, and the direction of the normal vector is determined by taking the difference between the top and bottom points and normalizing to a unit vector, as illustrated in Fig. 18. As the configuration of the shell evolves in time, the direction of each of the eight normal vectors is updated as described in the next subsection.

Given the normal vector, an arbitrary point  $\pi = (\xi, \eta, \zeta)$  inside the shell is transformed to  $p$  in  $(x, y, z)$  coordinates as follows:

$$p = \sum_{i=1}^8 w_i(\xi, \eta) \left( p_i + \zeta \frac{t_i}{2} n_i \right) \quad (23)$$

The first component inside the bracket,  $p_i$ , corresponds to Eq. 21 above representing the midsurface of the shell. The second component, involving  $\zeta$ , translates the displacement along the  $\zeta$  axis back into  $(x, y, z)$  coordinates.

### 5.4 The normal-vector coordinate system

The normal vectors will play a crucial part in our model. For example, in Sect. 5.6, we assume that the material of the paper is completely flexible and offers no resistance to external forces in the direction perpendicular to it. Because of this, and to assist in updating the normal vectors from one configuration of the paper to the next, we establish a coordinate system at each reference point based on the direction of the normal at that point.

For this normal-vector coordinate system at reference point  $i$ , we use the notation  $\hat{x}_i, \hat{y}_i, \hat{z}_i$ . The new  $z$  axis is in the direction of the normal to the surface at that reference point,  $n_i$ . The new  $x$  axis is in a direction perpendicular to both this new  $z$  axis and the *old*  $y$  axis, that is, the  $y$  axis of the original global  $x, y, z$  coordinates. This direction is  $e^y \times e_i^{\hat{z}}$ , where  $e^y$  is a unit vector along the global  $y$  axis, and  $e_i^{\hat{z}}$  is a unit vector along the new  $z$  axis, which is in the same direction as

$\mathbf{n}_i$ . (A degenerate case arises when the normal  $\mathbf{n}_i$  coincides with the direction of the global  $y$  axis, in which case, we set the new  $x$  axis to be in the direction of the old  $z$  axis.) Having established the new  $z$  and  $x$  axes, the new  $y$  axis is set to be perpendicular to them both, that is, in the direction  $\mathbf{e}_i^{\hat{z}} \times \mathbf{e}_i^{\hat{x}}$ .

We now consider how to update the normal vector  $\mathbf{n}_i$  from one moment to the next. We assume that the new normal is the result of rotating  $\mathbf{n}_i$  through an angle  $\alpha_i$  around the  $\hat{x}_i$  axis and an angle  $\beta_i$  around the  $\hat{y}_i$  axis. Then the new normal vector is

$$\begin{aligned} \mathbf{n}'_i &= \mathbf{e}_i^{\hat{x}} \sin \beta_i + \mathbf{e}_i^{\hat{y}} \cos \beta_i \sin(-\alpha_i) + \mathbf{e}_i^{\hat{z}} \cos \beta_i \cos(-\alpha_i) \\ &= \beta_i \mathbf{e}_i^{\hat{x}} - \alpha_i \mathbf{e}_i^{\hat{y}} + \mathbf{e}_i^{\hat{z}} \end{aligned} \tag{24}$$

assuming that the rotations are small.  $\mathbf{n}'_i$  will be the  $\hat{z}$  direction of the normal-vector coordinate system that is used for the next step.

The angles  $\alpha_i$  and  $\beta_i$  are central to the updating procedure, and will figure prominently in what follows.

### 5.5 Displacement

If the position of point  $\mathbf{p}$  at time  $h$  is  $\mathbf{p}$ , and at time  $h + \Delta h$  is  $\mathbf{p}'$ , its displacement from time  $h$  to time  $h + \Delta h$  in the  $x$ ,  $y$  and  $z$  directions is

$$\mathbf{d} = \mathbf{p}' - \mathbf{p}$$

by substituting the value of  $\mathbf{p}$  according to Eq. 23,

$$\mathbf{d} = \sum_{i=1}^8 w_i(\xi, \eta) \left\{ (\mathbf{p}'_i - \mathbf{p}_i) + \zeta \frac{t_i}{2} (\mathbf{n}'_i - \mathbf{n}_i) \right\}$$

We write  $\mathbf{d} = (u, v, w)$ . The entire displacement of node  $i$  from time  $h$  to  $h + \Delta h$  is characterized by the following 5-vector:

$$\mathbf{q}_i = (u_i, v_i, w_i, \alpha_i, \beta_i)$$

where  $u_i, v_i,$  and  $w_i$  are the displacements of  $\mathbf{p}_i$  in the  $x, y$  and  $z$  axis directions respectively, and  $\alpha_i$  and  $\beta_i$  are the rotation angles around the  $\hat{x}$  and  $\hat{y}$  axes, respectively.

Given the displacement vectors  $\mathbf{q}_i$  for each of the nodes of a surface patch, we now calculate the displacement vector  $\mathbf{d}$  for a general point on the patch at position  $(\xi, \eta, \zeta)$ .

$$\begin{aligned} \mathbf{d} &= \sum_{i=1}^8 w_i(\xi, \eta) \left\{ (\mathbf{p}'_i - \mathbf{p}_i) + \zeta \frac{t_i}{2} (\mathbf{n}'_i - \mathbf{n}_i) \right\} \\ &= \sum_{i=1}^8 w_i(\xi, \eta) \left\{ \begin{bmatrix} u_i \\ v_i \\ w_i \end{bmatrix} + \zeta \frac{t_i}{2} (\beta_i \mathbf{e}_i^{\hat{x}} - \alpha_i \mathbf{e}_i^{\hat{y}}) \right\} \\ &= \sum_{i=1}^8 \mathbf{w}_i \mathbf{q}_i \end{aligned} \tag{25}$$

where the interpolation matrix for reference point  $\mathbf{p}_i$  is

$$\mathbf{w}_i = w_i(\xi, \eta) \begin{bmatrix} 1 & 0 & 0 & -\zeta \frac{t_i}{2} l_i^{\hat{y}} & \zeta \frac{t_i}{2} l_i^{\hat{x}} \\ 0 & 1 & 0 & -\zeta \frac{t_i}{2} m_i^{\hat{y}} & \zeta \frac{t_i}{2} m_i^{\hat{x}} \\ 0 & 0 & 1 & -\zeta \frac{t_i}{2} n_i^{\hat{y}} & \zeta \frac{t_i}{2} n_i^{\hat{x}} \end{bmatrix}$$

and  $\mathbf{e}_i^{\hat{x}} = (l_i^{\hat{x}}, m_i^{\hat{x}}, n_i^{\hat{x}}), \mathbf{e}_i^{\hat{y}} = (l_i^{\hat{y}}, m_i^{\hat{y}}, n_i^{\hat{y}})$ .

We have now completed our analysis of the geometry of the surface element or patch. In order to summarize: each patch is situated in three-dimensional space by the coordinates of its eight reference points  $\mathbf{p}_i$ . A local coordinate system is defined for the patch which allows any point within it to be defined by coordinates  $(\xi, \eta, \zeta)$ . The entire volume of the patch is swept out as these coordinates range from  $-1$  to  $1$ . The third coordinate corresponds to the thickness of the patch, and  $\zeta = 0$  defines the midsurface. Eight of the nine combinations of the values  $-1, 0, 1$  for each of  $\xi$  and  $\zeta$  define the eight reference points  $\mathbf{p}_i$  (the ninth,  $(0, 0)$ , is the center of the patch). Any point  $\boldsymbol{\pi} = (\xi, \eta, \zeta)$  within the patch can be expressed in terms of its global coordinates  $\mathbf{p} = (x, y, z)$  using the transformation of Eq. 23. This transformation also involves the normal vector  $\mathbf{n}_i$  to the patch at each reference point.

The normal vector  $\mathbf{n}_i$  is used to define a coordinate system at reference point  $i$  which will be deployed in the analysis below. As the patch moves from one configuration to the next under the influence of forces discussed in subsequent sections, it is necessary to update the coordinates of each reference point and the orientation of the normal vector at each one. The key to the updating procedure is the displacement vector, a five-dimensional vector  $\mathbf{q}_i$  which includes the displacement of the reference point in the  $x, y$  and  $z$  directions, as well as the angular displacements around the two axes of the normal-vector coordinate system, which are perpendicular to the normal at the reference point. Given any point within the patch expressed as  $(\xi, \eta, \zeta)$  in local coordinates, and the five-dimensional displacement vectors  $\mathbf{q}_i$  for each reference point, expression (25) shows how to calculate the corresponding displacement of the point in global  $(x, y, z)$  coordinates. These displacements occur as the result of the forces that we discuss next.

### 5.6 Stress

*Stress* ( $\boldsymbol{\sigma}$ ) measures the distribution of the internal forces in the shell, and determines the material's resistance to deformation under the pressure of external forces ( $\mathbf{b}$ ). The stress at any point within the shell—and here, we are considering a general point  $\mathbf{p}$  within a surface element, not a reference point  $\mathbf{p}_i$ —is defined as the force per unit area over a small area ( $\Delta A$ ) of the body. Formally,

$$\boldsymbol{\sigma} = \lim_{\Delta A \rightarrow 0} \frac{\Delta \mathbf{b}}{\Delta A}$$

Stress can be resolved into normal stress and shear stress [16,21]. The former measures the force perpendicular to the surface, while the latter measures the forces that act parallel to the surface. For example,  $\sigma_x$  is a stress perpendicular to the  $yz$  plane, while  $\sigma_{xy}$  and  $\sigma_{xz}$  are stresses in the  $yz$  plane that are parallel to the  $y$  and  $z$  axes, respectively. A total of six stresses act at every point within the shell, and we express them as a column vector  $\boldsymbol{\sigma} = [\sigma_x, \sigma_y, \sigma_z, \sigma_{xy}, \sigma_{xz}, \sigma_{yz}]^T$ .

The effect of stress is to deform the body under consideration. The amount of deformation is called *strain*, and is expressed as the change in length per unit of the original length. Each of the six stresses at a point (more precisely, at a vanishingly small area) causes a corresponding amount of strain, where strain is a six-dimensional vector that corresponds to the spatial derivatives of the point's displacement  $\boldsymbol{d} = \boldsymbol{p}' - \boldsymbol{p}$  discussed earlier:

$$\boldsymbol{\epsilon} = \begin{bmatrix} \epsilon_x \\ \epsilon_y \\ \epsilon_z \\ \epsilon_{xy} \\ \epsilon_{xz} \\ \epsilon_{yz} \end{bmatrix} = \begin{bmatrix} \frac{\partial}{\partial x} & 0 & 0 \\ 0 & \frac{\partial}{\partial y} & 0 \\ 0 & 0 & \frac{\partial}{\partial z} \\ \frac{\partial}{\partial y} & \frac{\partial}{\partial x} & 0 \\ \frac{\partial}{\partial z} & 0 & \frac{\partial}{\partial x} \\ 0 & \frac{\partial}{\partial z} & \frac{\partial}{\partial y} \end{bmatrix} \boldsymbol{d}$$

The relationship between the degree of stress and the amount of strain it causes is given by Hooke's law of elasticity, which states that the amount by which a body is deformed—the strain—is directly proportional to the stress that cause the deformation. The stress–strain relation can be expressed by the equation

$$\boldsymbol{\sigma} = \boldsymbol{D}\boldsymbol{\epsilon}, \tag{26}$$

where  $\boldsymbol{D}$  is the deformation matrix, discussed below. First, however, we consider the problem of calculating the strain itself.

### 5.7 Calculating the strain

The strain is obtained by taking partial derivatives of  $\boldsymbol{d}$  with respect to the global coordinates  $x$ ,  $y$  and  $z$ , as shown above. Equation 25 expresses the displacement at any point within a patch in terms of its local  $(\xi, \eta, \zeta)$  coordinates and the eight vectors  $\boldsymbol{q}_i$  that characterize the displacement of each reference point of the patch. Taking the derivatives of this equation with respect to  $\xi$ ,  $\eta$  and  $\zeta$  is a simple matter. In order to calculate the strain, partial derivatives with respect to  $x$ ,  $y$  and  $z$  must be expressed in terms of partial derivatives with respect to  $\xi$ ,  $\eta$  and  $\zeta$ .

This is done by applying the chain rule in the following form:

$$\begin{bmatrix} \frac{\partial}{\partial x} \\ \frac{\partial}{\partial y} \\ \frac{\partial}{\partial z} \end{bmatrix} = \boldsymbol{J}^{-1} \begin{bmatrix} \frac{\partial}{\partial \xi} \\ \frac{\partial}{\partial \eta} \\ \frac{\partial}{\partial \zeta} \end{bmatrix} \tag{27}$$

where  $\boldsymbol{J}^{-1}$  is the inverse of the Jacobian matrix that relates local coordinate derivatives to global ones:

$$\boldsymbol{J} = \begin{bmatrix} \frac{\partial x}{\partial \xi} & \frac{\partial y}{\partial \xi} & \frac{\partial z}{\partial \xi} \\ \frac{\partial x}{\partial \eta} & \frac{\partial y}{\partial \eta} & \frac{\partial z}{\partial \eta} \\ \frac{\partial x}{\partial \zeta} & \frac{\partial y}{\partial \zeta} & \frac{\partial z}{\partial \zeta} \end{bmatrix} \tag{28}$$

$\boldsymbol{J}$  can be determined by taking derivatives of Eq. 23 above, which gives an explicit transformation from local coordinates to global ones. The details can be found in the Appendix.

The upshot is that the strain  $\boldsymbol{\epsilon}$  at any point can be obtained from its local coordinates  $\xi$ ,  $\eta$  and  $\zeta$  and the displacement vector  $\boldsymbol{q}_i$  at each of the patch's eight reference points. The operation can be summarized in matrix form as

$$\boldsymbol{\epsilon} = \sum_{i=1}^8 \boldsymbol{B}_i(\xi, \eta, \zeta) \boldsymbol{q}_i \tag{29}$$

where  $\boldsymbol{B}_i(\xi, \eta, \zeta)$ , the *strain-displacement matrix*, can be obtained explicitly using the above techniques, for each reference point  $i$ .

### 5.8 The deformation matrix

If a body is compressed, then it tends to expand sideways; on the other hand, if it is pulled, then the material contracts laterally [16,21]. These effects are quantified by the deformation matrix  $\boldsymbol{D}$  that characterizes the relationship between stress and strain expressed by Eq. 26.

The deformation matrix depends on three constants that characterize the material under consideration: Young's modulus of elasticity  $E$ , Poisson's ratio  $\nu$ , and the shear correction factor  $K$ . Young's modulus represents the stiffness of the material. Poisson's ratio captures the relation between deformation in the direction of the stress and deformations in directions perpendicular to it (we assume that the material is isotropic).

The shear correction factor is used to model a shear strain that is not uniform throughout the material, and allows the strain to alter linearly across its thickness. In our simulations, we typically use values of  $E = 1,370 \text{ N cm}^{-1}$ ,  $\nu = 0.33$ , and  $K = \frac{5}{6}$  for paper with mass density of  $80 \text{ m}^{-3}$  [1].

We assume that the shell does not resist any deformation in the  $\hat{z}$  direction, so that the stress normal to its surface is zero. In the normal-vector coordinate system, the deformation matrix at point  $\boldsymbol{\pi} = (\xi, \eta, \zeta)$  is

$$\hat{\boldsymbol{D}} = \begin{bmatrix} \frac{E}{1-\nu^2} & \frac{E\nu}{1-\nu^2} & 0 & 0 & 0 & 0 \\ \frac{E\nu}{1-\nu^2} & \frac{E}{1-\nu^2} & 0 & 0 & 0 & 0 \\ 0 & 0 & 0 & 0 & 0 & 0 \\ 0 & 0 & 0 & \frac{E}{2(1+\nu)} & 0 & 0 \\ 0 & 0 & 0 & 0 & \frac{EK}{2(1+\nu)} & 0 \\ 0 & 0 & 0 & 0 & 0 & \frac{EK}{2(1+\nu)} \end{bmatrix} \tag{30}$$

This matrix must be transformed to give a deformation matrix  $\mathbf{D}$  in the global coordinate system. The elements of the transformation matrix  $\mathbf{Q}$  are obtained from the direction cosines of the  $\hat{x}$ ,  $\hat{y}$ ,  $\hat{z}$  coordinate axes at point  $\mathbf{p}$  measured in the  $x$ ,  $y$ ,  $z$  coordinate directions.  $\mathbf{Q}$  transforms the strain vector in local coordinates  $[\epsilon_\xi, \epsilon_\eta, \epsilon_\zeta, \epsilon_{\xi\eta}, \epsilon_{\xi\zeta}, \epsilon_{\eta\zeta}]^T$  into the strain vector in global coordinates  $[\epsilon_x, \epsilon_y, \epsilon_z, \epsilon_{xy}, \epsilon_{xz}, \epsilon_{yz}]^T$ . Again, the details are relegated to the Appendix.

### 5.9 Effect of forces

The deformation of any element is determined by the external and internal forces that work on it. By using the principle of conservation of energy, we can translate the forces into the displacement of the element at time  $h + \Delta h$ . This section explains the principles, and the details are given in the Appendix.

When external forces are applied to a body, their potential energy ( $\delta E_T$ ) is converted into kinetic energy ( $\delta E_K$ ), corresponding to internal forces of inertia and damping, and potential energy ( $\delta E_P$ ), corresponding to stress. Conservation of energy is expressed by equating internal and external energy:

$$\delta E_K + \delta E_P = \delta E_T. \tag{31}$$

We begin with the external forces to which each element of the shell is subjected. There are three different types. *Body forces* ( $\mathbf{F}_B$ )—such as the force of gravity—apply throughout the element. *Surface forces* ( $\mathbf{F}_S$ ) may be applied at the surface of the shell—for example, the upper and lower surfaces of the left edge of the paper are held rigidly in place by forces exerted by the book’s spine. *Nodal forces* ( $\mathbf{R}_N$ ) are applied at individual reference points, for example by the user’s thumb and forefinger on the corner of the page as it is turned. These three examples—gravity, the spine, and the user’s effort in turning the page—are the only external forces in our simulation, although the model permits more general body, surface, and nodal forces to be applied.

Potential energy equals force times displacement. Each force must be integrated appropriately. The body force is integrated with respect to the element’s volume, yielding  $\mathbf{R}_B$ . The surface force is integrated with respect to its surface area, yielding  $\mathbf{R}_S$ . Both these forces, along with  $\mathbf{R}_N$ , are multiplied by the displacement to compute the energy.

The potential energy done by external forces is calculated by multiplying each vector by the displacement vector and summing:

$$\delta E_T = (\delta \mathbf{q})^T (\mathbf{R}_B + \mathbf{R}_S + \mathbf{R}_N)$$

Now, we turn to the internal forces of inertia, damping, and stress. *Inertial force* is caused by the element’s reluctance to accelerate or decelerate. In accordance with Newton’s second law, it is given by  $\rho \mathbf{w}\ddot{\mathbf{q}}'$ , where  $\rho$  is the element’s

mass density. *Damping force* results from friction within the deforming material, and is proportional to the element’s velocity:  $\kappa \mathbf{w}\dot{\mathbf{q}}'$  where  $\kappa$  is the element’s damping coefficient. *Stress* measures the material’s resistance to deformation due to the external forces and the element’s initial configuration, and can be written as  $\mathbf{D}\mathbf{B}\mathbf{q}' + \boldsymbol{\sigma}_0$ . All the three effects must be integrated over the volume of the element. This gives

$$\delta E_K + \delta E_P = (\delta \mathbf{q})^T (\mathbf{M}\ddot{\mathbf{q}}' + \mathbf{C}\dot{\mathbf{q}}' + \mathbf{K}\mathbf{q}' + \mathbf{S}_0)$$

The matrices  $\mathbf{M}$ ,  $\mathbf{C}$ , and  $\mathbf{K}$  are the element’s mass, damping, and stiffness matrices, respectively, and  $\mathbf{S}_0$  is the integrated initial stress  $\boldsymbol{\sigma}_0$ . If the initial position of the paper is flat, then  $\boldsymbol{\sigma}_0$  can be omitted altogether. For a more general case, where the paper might already be bent,  $\boldsymbol{\sigma}_0$  is not zero and is calculated in the same way as  $\boldsymbol{\sigma}$ .

The law of conservation of energy is expressed by equating  $\delta E_T$  with the sum of  $\delta E_K$  and  $\delta E_P$ . Canceling  $(\delta \mathbf{q})^T$  and moving  $\mathbf{S}_0$  to the other side yields the second-order differential equation

$$\mathbf{M}\ddot{\mathbf{q}}' + \mathbf{C}\dot{\mathbf{q}}' + \mathbf{K}\mathbf{q}' = \mathbf{R}_B + \mathbf{R}_S + \mathbf{R}_N - \mathbf{S}_0 \tag{32}$$

This is the fundamental equation that must be solved to determine how the position of the element evolves under the applied forces.

We solve this equation using Newmark implicit time integration [1, 18]. Given the position  $\mathbf{q}$ , velocity  $\dot{\mathbf{q}}$ , and acceleration  $\ddot{\mathbf{q}}$  of the element at time  $h$ , the new values  $\mathbf{q}'$ ,  $\dot{\mathbf{q}}'$  at time  $h + \Delta h$  are

$$\begin{aligned} \ddot{\mathbf{q}}' &= \frac{4}{\Delta h^2}(\mathbf{q}' - \mathbf{q}) - \frac{4}{\Delta h}\dot{\mathbf{q}} - \ddot{\mathbf{q}} \\ \dot{\mathbf{q}}' &= \dot{\mathbf{q}} + \int_h^{h+\Delta h} \ddot{\mathbf{q}} \, dh \end{aligned} \tag{33}$$

In order to determine the nodal displacement at time  $h + \Delta h$  based only on terms at time  $h$ , we substitute the value of  $\dot{\mathbf{q}}'$ ,  $\ddot{\mathbf{q}}'$  from Eq. 33 into Eq. 32 and then convert this into an expression for  $\mathbf{q}'$  by bringing all other terms to the right-hand side.

$$\begin{aligned} \mathbf{q}' \left[ \frac{4}{\Delta h^2} \mathbf{M} + \frac{2}{\Delta h} \mathbf{C} + \mathbf{K} \right] &= \mathbf{R}_B + \mathbf{R}_S + \mathbf{R}_N - \mathbf{S}_0 \\ &+ \mathbf{M} \left( \frac{4}{\Delta h^2} \mathbf{q} + \frac{4}{\Delta h} \dot{\mathbf{q}} + \ddot{\mathbf{q}} \right) \\ &+ \mathbf{C} \left( \frac{2}{\Delta h} \mathbf{q} + \dot{\mathbf{q}} \right) \end{aligned} \tag{34}$$

In order to summarize the entire algorithm to simulate the behavior of the element:

1. Initialize  $\mathbf{q}^0 = \dot{\mathbf{q}}^0 = \ddot{\mathbf{q}}^0 = 0$ .
2. Select the time step  $\Delta h$ .
3. Form the matrices  $\mathbf{M}$ ,  $\mathbf{C}$ ,  $\mathbf{K}$ ,  $\mathbf{S}_0$ .
4. For each time step:

- (a) Calculate the load  $R'_B, R'_S$ .
- (b) Calculate the displacement  $q'$  at time  $h + \Delta h$  according to the equation just mentioned.
- (c) Calculate the acceleration  $\ddot{q}'$  and velocity  $\dot{q}'$  at time  $h + \Delta h$  from Eq. (33).

## 6 Comparison of methods

Table 2 shows the essential features of the page-turning techniques, which we have surveyed. It contains entries for the two variants of the *peeling* technique, basic peeling and the use of a 3D correction to simulate foreshortening of the paper due to its extension in the  $z$  direction; two *geometric wrapping* techniques that involve wrapping the paper around a cylinder and cone, respectively; the basic *mass-spring model* and two variants that attempt to simulate more natural bending and twisting, respectively; and the *finite element* method, which models the paper as a 3D shell whose thickness is represented by a single element.

### 6.1 Time complexity

The computation time required for each method is largely dictated by the size of the grid, where applicable. Most methods use rectangular grids. However, the first method needs no grid, and the third mass-spring variant uses a triangular grid to resist twisting by constraining dihedral angles between neighboring triangles. Grid elements in the finite-element method are three dimensional, but are arranged in a two-dimensional array because paper is thin enough for a single layer of elements to adequately model its substance.

We simulated a complete page turn with each method, involving many intermediate postures between the beginning, where the page lies flat on the right-hand side, and the end, where it lies flat on the left-hand side. For the first four methods, which do not involve iteration.

Table 2 shows the average time taken to compute the configuration of the paper at each posture. For the last four methods, it shows the average number of iterations to reach a posture, and the average execution time per iteration. The execution time taken by these methods to compute the configuration of the paper at each posture is the product of these two numbers. The time taken to completely turn a page can be calculated by multiplying this product by the number of in-between postures—say 20 in-betweens—for a fast  $\frac{2}{3}$ -second page turn animated at 30 frames/s.

In each case, the lower right-hand corner of the page was constrained to move along the same arc. Each point is specified as a position on the grid. The number of possible positions with different  $x$ -values is twice the grid size. Times are shown for grids of size  $10 \times 10$  (18 postures between the paper lying flat on the right side and flat on the left side) and

$100 \times 100$  (198 in-between postures). The smaller grid gives a rough idea of what the page turn looks like, while the larger one produces a very good visual approximation of the page turn. In practice, one would not use a square grid but tailor it to the aspect ratio of the paper, using an  $8 \times 11$  or  $9 \times 11$  grid for  $8\frac{1}{2} \times 11$ '' paper. Our implementations are not optimized and could no doubt be improved by more careful attention to computational details. The code was written in Java, and timings were measured on a 2.8 GHz Pentium 4 processor.

The two-dimensional peeling technique does not use a grid and is essentially instantaneous; it takes  $50 \mu\text{s}$  to compute a posture. The second method, which incorporates a correction for foreshortening in the  $z$  direction, does require a grid, and this increases computation time from  $O(1)$  to  $O(n^2)$  for an  $n \times n$  grid. Table 2 gives values of 16 ms for the  $10 \times 10$  grid and 5.96 s for the  $100 \times 100$  grid, which are indeed on the order of 100 and 10,000 times the values for the  $O(1)$  peeling technique (to within a factor of 3 and 12, respectively).

The time taken by geometric wrapping is  $O(n)$  for the cylinder and  $O(n^2)$  for the cone. The difference is because in the former case each element of the paper has the same position for all values of  $z$ , while in the latter the position depends on the  $z$ -value, as described in Sect. 3. The time taken for the cylinder is 1 ms for the  $10 \times 10$  grid and 312 ms for the  $100 \times 100$  grid; the increase is rather more than the factor of 10 that is expected for an  $O(n)$  method but does include the time required to output the coordinates of all the points, which adds a small  $O(n^2)$  component. The time taken for the cone is 16 ms for the  $10 \times 10$  grid and 6.44 s for the  $100 \times 100$  grid.

Now, we turn to the physical simulation models in the lower half of the Table. Their stability depends on the value chosen for the integration time step. If this is too large, then the simulation will be unstable—the paper may vibrate, or, worse still, the computation may blow up and produce infinite values. Although the explicit time integration technique used for the first of these four physical models is the simplest method, it is less stable than the implicit methods that are used for the remaining three, and therefore requires smaller time steps. However, to compare the execution time based on the complexity of the model itself, we have chosen the same time step value of  $\Delta h = 20$  ms, which works well for all physical models.

For each method, the number of iterations required for the  $100 \times 100$  grid is far smaller than for the  $10 \times 10$  one because the previous posture of the page, which is used as a starting point for iteration, is far closer to the current posture on the finer grid. Recall that we are computing 18 in-between postures for the coarse grid and 198 for the fine grid.

Table 2 gives the *average* number of iterations. In physical models, the number of iterations required to reach a specified posture varies. More accurate models simulate the stiffness properties of the paper better, which means that there is little

**Table 2** Summary of page turning techniques

Technique	Method	Mesh	Time integration			Iteration/position			Time/iteration (s)			Time complexity
						$10 \times 10$	$100 \times 100$	$100 \times 100$	$10 \times 10$	$100 \times 10$	$100 \times 100$	
Peeling												
Two-dimensional	Produce dog-ear effect by simple geometric reflection	–	–	–	–	1	1	1	$5 \times 10^{-5}$	$5 \times 10^{-5}$	$5 \times 10^{-5}$	$O(1)$
With 3D correction	Adjust dog-ear with heuristic $z$ -value and spline correction	Rectangle	–	–	–	1	1	1	0.016	0.016	5.96	$O(n^2)$
Geometric wrapping												
Around cylinder	Map grid to cylinder whose radius and axis vary	Rectangle	–	–	–	1	1	1	0.001	0.001	0.31	$O(n)$
Around cone	Map grid to cone whose angle and apex vary	rectangle	–	–	–	1	1	1	0.016	0.016	6.44	$O(n^2)$
Mass-spring model												
Basic	Calculate spring lengths from Hooke's law and apply limit straining	Rectangle	–	–	–	349	27	27	0.016	0.016	6.38	$O(n^2)$
With bending	Apply Hooke's law for elongation, and calculate curvature for compression	Rectangle	–	–	–	386	30	30	0.015	0.015	6.38	$O(n^2)$
Bending, no twisting	Take account of bending energy by calculating dihedral angle between neighboring triangles	Triangle	–	–	–	450	33	33	0.017	0.017	6.94	$O(n^2)$
Finite element												
3D shell model	Use stress-strain relationship to derive the deformation from applied forces	3D patch	–	–	–	500	–	–	6.10	6.10	–	$O(n^4)$

**Table 3** Space complexity of page turning models

Technique	Stored vector	Space complexity
Peeling		
Two-dimensional	$(x, y)$	$O(1)$
With 3D correction	$(x, y, z)$	$O(1)$
Geometric wrapping		
Around cylinder	$(x, y, z)$	$O(1)$
Around cone	$(x, y, z)$	$O(1)$
Mass-spring model		
Basic	$(x, y, z)$	$O(n^2)$
With bending	$(x, y, z)$	$O(n^2)$
Bending, no twisting	$(x, y, z)$	$O(n^2)$
Finite element		
3D shell model	$(u, v, w, \alpha, \beta)$	$O(n^2)$

change from one iteration to the next. The largest change from one iteration to the next occurs when force is first applied to the page, and, therefore, only a small number of iterations are needed to reach the first given posture. When the page approaches its equilibrium posture near the end of the simulation, the page deformation reduces, the amount of change in each iteration decreases, and more iterations are required to reach a posture. In practice, the number of iterations ranges from about 200 steps below the average to 300 steps above it for the  $10 \times 10$  grid, and from about 10 steps below to 20 steps above for the  $100 \times 100$  grid.

In terms of the grid size, the complexity of the mass-spring models is  $O(n^2)$ . For all the three of them, the time taken for a complete 20-frame page turn animation is about  $400 \times 16 \times 20 \text{ ms} \approx 2 \text{ min}$  on a  $10 \times 10$  grid, and about  $30 \times 6.5 \times 20 \text{ s} \approx 1 \text{ h}$  on a  $100 \times 100$  one.

The finite element method is far more complex still, and grows with the fourth power of the grid size. A complete 20-frame page turn animation takes  $500 \times 6.1 \times 20 \text{ ms} \approx 17 \text{ h}$  even on the crude  $10 \times 10$  grid, and we are clearly unable to perform the computation for the larger  $100 \times 100$  grid because it would take on the order of  $10^4$  times as long.

Note that in a practical implementation many speed-ups are possible. The integration step size could be carefully tuned. Moreover, one could cache the results of a single page turn (or, perhaps, a selection of different page turns) and texture-map the actual contents of each page onto the cached geometric surface. We did, in fact, do this in an earlier project [8].

## 6.2 Space complexity

Table 3 shows the space complexity of the techniques, along with the vector representation they use. In all the cases, the initial positions of the four corners of the page must be stored.

Geometric models define the appearance of the page by a set of equations, each relating to a particular user action. In this article, we only consider the case where a user picks the bottom corner of the page and turns it from right to left. The page's appearance at any point is obtained by entering the current position of the bottom corner of the page into the appropriate geometric equation. Thus, the space complexity is  $O(1)$ .

In physical models, the paper is simulated by dividing its material into  $m \times n$  elements, and the new position of an element in the grid at time  $h + \Delta h$  is calculated from the element's current position at time  $h$ . In the mass-spring model, each element is treated as a particle whose position is given by a 3-vector  $(x, y, z)$ . At each time step, its position at time  $h$  must be stored; thus the space complexity is  $O(n^2)$ .

In finite element methods, the size and shape of the elements are taken into account. Each element is defined by eight reference points, and at each time step, the displacements of all reference points at time  $h$  are stored. The displacement of  $\mathbf{p}_i$  at any given time is represented by a 5-vector  $(u_i, v_i, w_i, \alpha_i, \beta_i)$ , where  $u_i, v_i,$  and  $w_i$  are the displacement of  $\mathbf{p}_i$  in the  $x, y,$  and  $z$  directions, and  $\alpha_i$  and  $\beta_i$  are the rotation angles around the  $x$  and  $y$  normal-vector coordinate axes. Again, the space complexity is  $O(n^2)$ .

## 6.3 Visual fidelity

Figures 19 and 20 show the visual appearance of the page produced by each method when the lower right-hand corner of the page is placed at three different positions. In order to achieve this in a geometric simulation, the program is given the desired  $(x, y, z)$  coordinates of the page corner—in the case of the two-dimensional peeling method, just the  $(x, y)$  coordinates. For physical models, it involves applying a sequence of forces to the lower right-hand corner of the page which are sufficient to bring it to the appropriate point.

Figure 19 shows representative samples of the visual effects produced by the geometric techniques of peeling and wrapping. Figure 19a is clearly inferior to 19b because, as explained in Sect. 2, the creased dog-ear has exactly the same area as the part of the page beneath, which has been revealed, and which is obviously unnatural. Nevertheless, when used in a reactive real-time page-turning simulation users do not, in practice, notice this deficiency. The geometric wrapping models in Fig. 19c,d do not fare well. The cylindrical model (Fig. 19c) looks rather unnatural. The first and third images of the conical model (Fig. 19d) suffers from the fact that the cone's axis is constrained to lie on the negative  $y$ -axis, and the page is therefore hardly curled at all. No doubt different variants of this model could produce more realistic effects.

Some more radical differences can be seen in the images in Fig. 20 produced by the physical methods—three mass-spring models of increasing complexity and the finite ele-

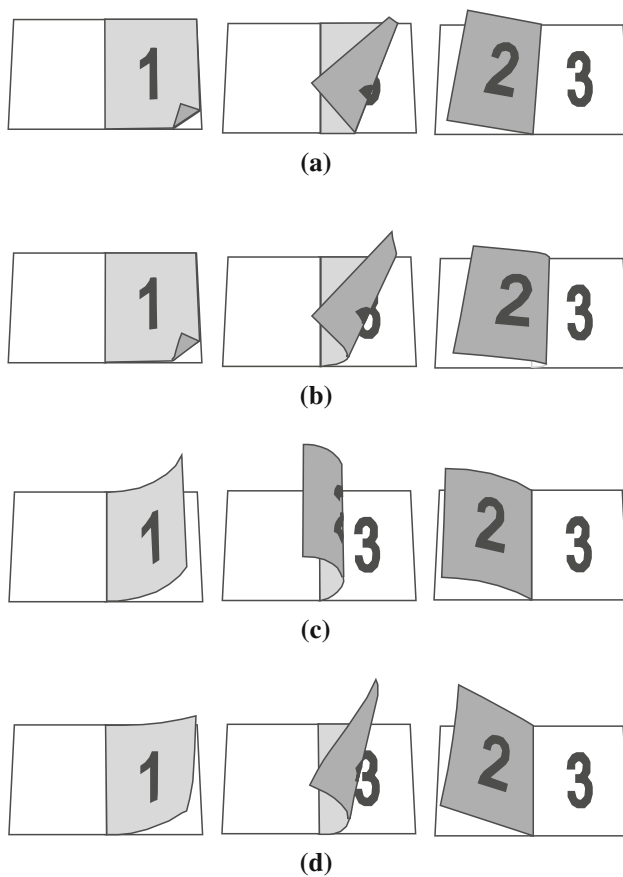


**Fig. 19** Geometric page turning simulation using: **a** peeling 2D, **b** peeling 3D, **c** cylindrical, **d** conical models

ment method. Because the basic mass-spring method does not model the page's resistance to bending forces well, the page crumples in a way that resembles cloth rather than paper, weighed down by the force of gravity. This can be seen in Fig. 20a. In Fig. 20b the page is twisted unnaturally, an effect which—although it looks plausible—is impossible to achieve with ordinary paper. The third model tries to correct this twist and overall the simulation looks reasonably natural, but a slight twist can still be discerned in the third image of Fig. 20c. This twisting behavior does not appear in the finite element method (Fig. 20d), which looks quite natural.

## 7 User study<sup>1</sup>

Previous sections explained several computer graphic techniques for modeling the act of turning a page, and compared their performance in terms of computation time and visual fidelity. We now describe an evaluation study designed to determine whether book models with realistic page turning

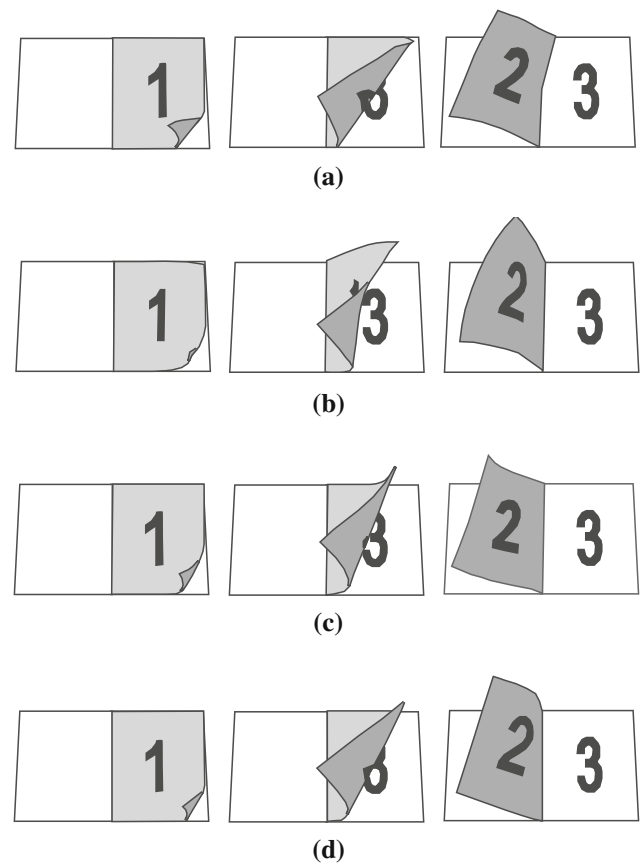


**Fig. 20** Physical page turning simulation using: **a** basic mass-spring, **b** bending, **c** bending without twisting, **d** finite element method models

offer real advantages over conventional document representations like Adobe PDF readers, HTML browsers, and physical books.

In order to study the impact of a realistic book model on the user's reading performance and satisfaction, we implemented a lightweight Adobe Flash-based system that uses the two-dimensional geometric page-turning technique. As noted in Sect. 6.3, different degrees of visual accuracy can readily be observed when simulation results are placed side by side as in Figs. 19 and 20. However, these effects generally go unnoticed when the images are viewed individually, particularly when they are animated under the control of a user who is focused on the page content. Slightly increased visual accuracy is vastly outweighed by the system's interactive response time.

In order to determine whether the new format can enhance a user's online reading experience, we developed a task based evaluation scheme and performed a user-centered comparison with books displayed in HTML and PDF format, and with physical books. We assessed the performance of each format in terms of *efficiency*, the time spent by the reader in answering each question, *effectiveness*, the number of questions answered correctly, and *reading experience*, a sub-

<sup>1</sup> Elements of this study were reported in Liesaputra and Witten [15].

jective assessment of usefulness, engagement, likeability, and ease of use.

The navigation functions used by participants to complete the task were also observed.

Participants found these tasks quite demanding. Consequently, we decided to perform two separate studies: the page-turning book model against the HTML and PDF formats, and (separately) against physical books. These are described in Sects. 7.4 and 7.5.

### 7.1 Using the book model

The page-turning mechanism is reasonably realistic and responds instantly to user actions. It uses the book metaphor to capture important characteristics of printed documents. The books have front and back covers (Fig. 21a,b), a title page, hyperlinked Table of Contents entries (Fig. 21c,d), and main text (Fig. 21e–g). The page edges on both sides of an open book indicate visually the length of the document and the reader's position in it. Hovering over the page edge reveals the page number as tooltip text.

Book pages are flexible, but the covers are rigid. For pages, we use the peeling technique described in Sect. 2. The act of turning the rigid cover is modeled using a shear transformation, where the shear angle increases as the cover begins to turn and decreases as it approaches its final position.

Readers grasp a page by depressing the mouse button anywhere along the page border. The page follows the movement of the mouse. Depending on where the button is released, the page either falls back to its original position or falls to the turned position. Right-hand pages turn automatically when the page is clicked or the right arrow key is depressed, and similarly with left-hand ones. The cover's inside border is visible when the book is open; clicking it closes the book.

Facilities are provided for nonsequential navigation. Users can jump to a beginning of a chapter or section by clicking its Table of Contents entry. Books may have tabs protruding from the page edges to mark the beginning of each section, or, alternatively, the location of figures.

Hovering over a tab reveals its page number and the section title or figure caption. If the reader clicks a page edge or tab, the books open to that page. If it is just few pages away from the current page, pages are turned one by one as if by an invisible hand. Otherwise, books open immediately at the new page.

Figure 21h shows the reader's controls. Using the right-click menu, the reader can switch the tabs to mark illustrated pages instead of chapter openings. The control bar (optionally) shown beneath the book allow users to access by page number, magnify the display, print the page, and rapidly turn page after page.

### 7.2 Document displays

Books used for this evaluation are presented in three electronic formats: HTML, PDF, and page-turning. In each case, they begin with a hyperlinked Table of Contents, followed by the main text.

In the HTML representation, shown in Fig. 22, readers can click on section names and return to the Table of Contents by scrolling to the top or pressing the browser's *back* button.

The standard Adobe Reader application was used to view PDF documents. It opens in thumbnail view, and participants can access any page by clicking its thumbnail in the panel on the left or entering its page number in the control bar at the top. They can page sequentially through documents using the scrollbar, arrow keys, or by clicking *next* and *previous* button in the control bar. They can switch from thumbnail to bookmark view.

Figure 23 shows these two views. The beginning of each section is bookmarked, so the bookmark view provides an ever-present Table of Contents adjacent to the page currently being read. Readers can go to a section by clicking its bookmark or its link in the Table of Contents.

With the page-turning model, shown in Fig. 21, users navigate by turning pages with the mouse, arrow keys, or by clicking on *next* and *previous* buttons in the control bar beneath the book. They can go to a page by clicking its edge or entering its number in the control bar. Sections can be accessed by clicking their bookmark tab or through the link on the Table of Contents page. Similarly, participants return to the Table of Contents by clicking its tab.

In order to ensure that the document layout does not affect the evaluation, all formats (except HTML) were paginated in exactly the same way. Physical books were created by printing the paginated documents in color, double-sided, and stapling down the left-hand side.

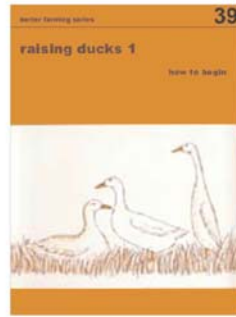
### 7.3 Procedure

We recruited 24 university students aged 20–40 from a variety of disciplines, who had used computers extensively for several years and were already familiar with HTML and PDF documents. None had used the page-turning system.

Subjects came individually to the study and completed a profiling questionnaire that recorded age range, gender, language proficiency, and their experience with computers, web browsers and the Adobe Reader.

In order to ensure that they could navigate freely, subjects were asked to browse a book in each format. We explicitly demonstrated any navigation functions that they did not appear to know. For example, most were unaware of PDF's bookmark view or that they could go to a page in the book model by clicking on its edge as well as its bookmark tab. Overall, subjects found the book model natural and needed

**Fig. 21** *Raising Ducks: How to Begin* book: **a, b** opening the front cover, **c, d** turning the Table of Contents page, **e, g** turning another page, **h** the right-click menu and control bar



(a)



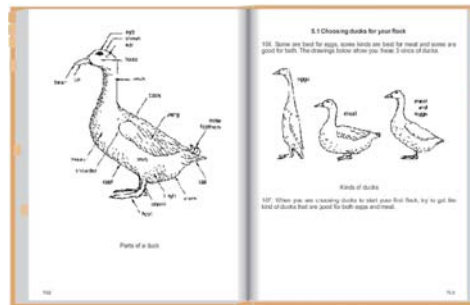
(b)



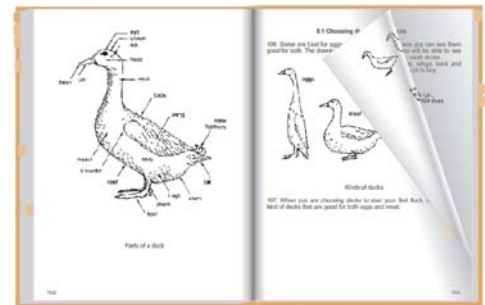
(c)



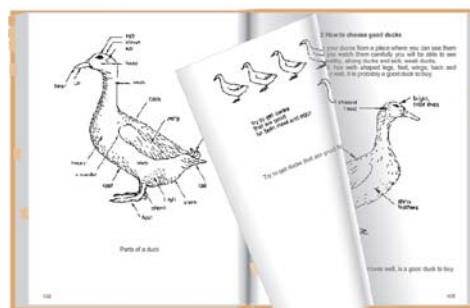
(d)



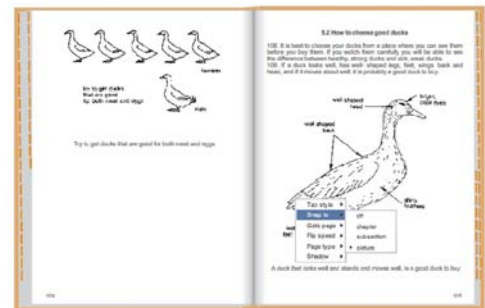
(e)



(f)



(g)



(h)

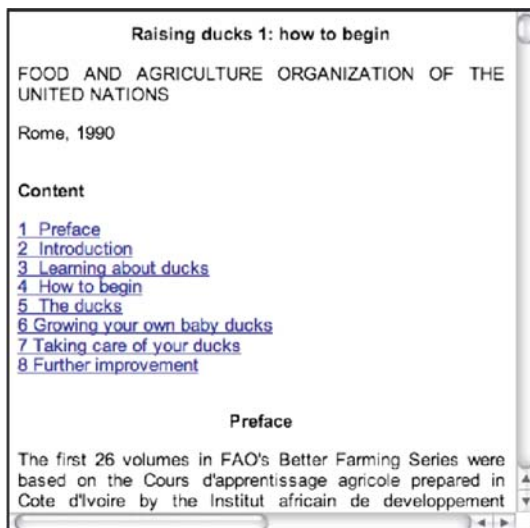


Fig. 22 *Raising Ducks: How to Begin* in HTML format

no more time to familiarize themselves with it than with the other formats.

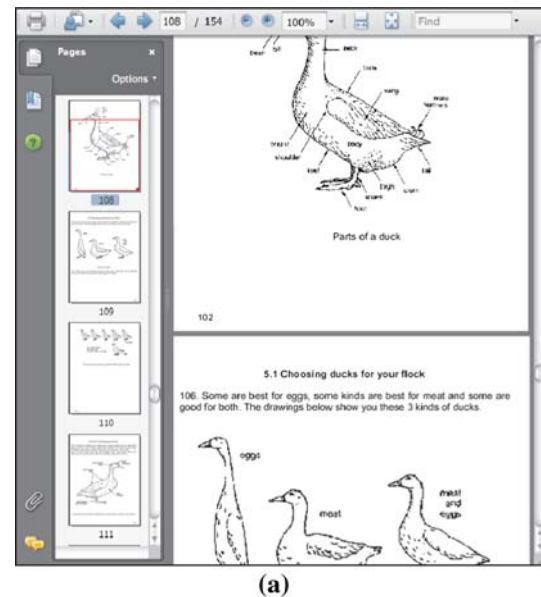
Participants were then given the books, one by one. Their task was to answer six multiple-choice questions seeking information in the document:

1. What kind of a book is it?
2. Which of the following would make the best title for the book?
3. Who do you think this book was written for?
4. From the following list of topics, write the section numbers that explain the topic.
5. Put a check next to each topic discussed in the book.
6. Put a check next to each statement that reflects the underlying beliefs or point of view of the book.

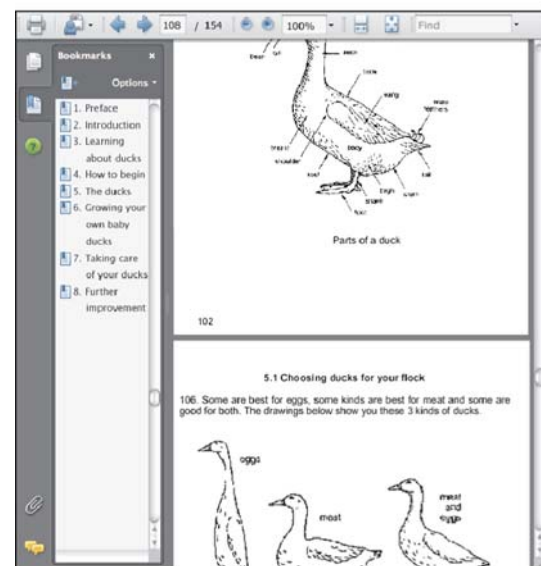
The first three are aimed at determining whether the participant understands what the book is about, and could be answered from the front matter and introductory section. The remainder aim to assess comprehension, and require participants to study the book thoroughly. Users were unlikely to know the answers already. They often needed to browse more than one section to find the answer, and then draw a conclusion. They were allowed to view the book while answering these questions.

Because the purpose of the study was to evaluate the experience of browsing visually through the text, participants were asked not to use *find* commands. In order to ensure that they felt no pressure and worked at their own pace, they did not know they were being timed. Functions they used during the task were recorded.

Having completed all the tasks, subjects completed a questionnaire to capture their opinions. They had to choose which



(a)



(b)

Fig. 23 *Raising Ducks: How to Begin* in PDF format with **a** thumbnail and **b** bookmark view

formats were relevant and useful for them, easier to navigate and use, easier to locate information, more pleasant and engaging to use, and finally which they preferred overall. They were asked to explain their choices and state which features they liked and disliked, as well as suggest improvements.

#### 7.4 Study 1: Page-turning versus HTML and PDF

We used three simple books: a history book (*History of the United States Told in One Syllable Words*), a children's book

(*Alice's Adventures in Wonderland*), and a handbook (*Raising Ducks: How to Begin*). Each book contains about a hundred pages (ranging from 80 to 140) and is divided into 8–18 chapters (some of which have subsections).

The history book represents a nonfiction work or textbook, where readers need to concentrate and read carefully. The children's book represents the kind of fiction that people read for leisure. The handbook is factual; it demands more attention than a children's book but less than a textbook.

Each subject read the books in the same order. They were exposed to each of three formats, a different one for each book. For example, one participant read Book 1 in HTML format, Book 2 in PDF format, and Book 3 in page-turning format. The six possible orderings were allocated evenly between participants: eight subjects read each book using the same document representation.

## 7.5 Study 2: Page-turning versus physical book

For the second study, we used two 10-chapter biographies from the Internet Archive: *Pavlova: A Biography* (184 pages) and *Princess Mary: A Biography* (254 pages). As before, each subject read the books in the same order: again there were eight participants for each combination of book and document format. Only 16 subjects were required; all had participated in the earlier study and so were familiar with the page-turning model.

## 7.6 Results

In general, participants adopted similar navigation strategies regardless of their background. (Note, however, that all had used computers and read documents in Web browsers or PDF readers for over 5 years.) No differences in navigation behavior and performance were observed between participants with 6 years' computing experience and ones with over 10 years' experience.

In terms of educational background, participants from Management, Art and Social Studies backgrounds had different reading strategies than those from Computer Science and Engineering. Having found a chapter they thought relevant, most members of the former group skim-read it to determine which parts were relevant before perusing it intensively to find the answer. On the other hand, most members of the latter group immediately read the chapter intensively. This apparent difference in reading behavior did not influence performance, which was only materially affected by the document representation.

We evaluate the participants' performance in terms of efficiency, effectiveness and subjective reading experience.

**Table 4** Average time (in seconds) to answer each question

	HTML	PDF	Book
(a) First user study			
Children's book	137 ± 36	78 ± 49	74 ± 56
Handbook	278 ± 173	173 ± 93	92 ± 68
History book	305 ± 150	219 ± 145	107 ± 77
	Simulated book		Physical book
(b) Second user study			
Anna Pavlova	283 ± 13		281 ± 15
Princess Mary	264 ± 19		279 ± 15

### 7.6.1 Efficiency

Table 4 shows the average time spent by participants in answering each question, expressed as mean ± standard deviation. Averages range from just over 1 to 5 min.

In the first user study, we found that participants answered questions faster using the page-turning model than the other two formats. A one-way analysis of variance of the times in Table 4a shows that the differences due to document format are statistically significant at the 5% level. The difference between the page-turning model and its closest competitor (PDF) are statistically significant at the 5% level for the history book, and at the 10% level for the other two.

Most participants found answers faster with the children's book. We observed that, for this book, they referred back to the Table of Contents at most twice to answer each question, whereas for the other two they referred back at least three times. When questioned, they explained that they could recall approximately which sections in the children's book were relevant to each question because they had already read or heard the story. The other books were new, and subjects were unfamiliar with their structure and content. Participants spent longer seeking the answers in the history book because it contains more information than the handbook.

There was a large variation between questions. In the first user study (Table 4a), time per question ranged from 3 s to 2 min for the first three questions and 1–14 min for the remainder. In the second (Table 4b), the range was 1 s to 2 min for the first three questions and 1–16 min for the remainder.

There was little variation in the time between participants in the second experiment. We suggest that this is because our subjects had become more fluent navigating the page-turning format during the first study. A one-way analysis of variance of the data in Table 4b shows no significant difference for either book at the 5% level (although for the second book the difference is significant at the 10% level).

Subjects worked faster with the second book than the first because it was better structured. They commented that since its contents were ordered by time, they could guess the loca-

**Table 5** Average number of correct answers (in %)

	HTML	PDF	Book
(a) First user study			
Children's book	90 ± 10	84 ± 9	86 ± 8
Handbook	85 ± 14	86 ± 19	81 ± 21
History book	74 ± 13	75 ± 12	78 ± 13
	Simulated book		Physical book
(b) Second user study			
Anna Pavlova	75 ± 14		77 ± 13
Princess Mary	79 ± 14		78 ± 18

tion of relevant passages based on the time of the event. In contrast, the first book was ordered by chapter author, and participants had to examine more than one chapter to gain complete information about a particular event.

### 7.6.2 Effectiveness

Table 5 gives the average number of questions that participants answered correctly in the two user studies. Most failed on the last two questions, for which it is necessary to locate information throughout the text and draw appropriate conclusions. We observed that some subjects did not attempt to find all the relevant text before answering the question: they drew conclusions from partial information. As with the efficiency measure, performance with the history book was noticeably inferior to the other two books in the first study, and performance with *Anna Pavlova* was inferior to that with *Princess Mary* in the second.

A one-way analysis of variance found no significant differences due to document format. From Tables 4 and 5, we conclude that while document format does not affect the level of comprehension, it does affect the time that readers require to process text. This is in line with many earlier studies [10, 11, 14, 17].

### 7.6.3 Reading experience

Once participants had completed all tasks, they were asked which formats were most useful, easy to navigate and locate information, pleasant and engaging, and preferred overall. They were allowed to choose more than one format. Table 6 summarizes their opinions.

Most readers commented that while HTML suffices for short documents, they prefer PDF or the page-turning model for long ones because the pagination breaks up the flow of information and helps them remember where things are in terms of their physical position on the page, allowing them to concentrate on searching rather than navigating. All subjects judged the page-turning book to be the format that is

**Table 6** Format preferences (in %)

Criteria	HTML	PDF	Book
(a) First user study			
Useful	0	17	83
Easy to navigate	0	33	100
Easy to locate information	0	0	100
Pleasant and engaging	0	0	100
Preferred	0	17	83
Criteria	Simulated book	Physical book	
(b) Second user study			
Useful	88	100	
Easy to navigate	100	88	
Easy to locate information	100	100	
Pleasant and engaging	100	100	
Preferred	88	83	

most engaging, natural and intuitive. However, 17% of participants preferred PDF because of their previous experience with it.

The second user study found little difference between the page-turning book and physical books. Participants said that both gave a similar reading experience but the former had the advantage of hyperlinks, allowing them to jump more quickly between the book's sections. In the physical book, they used the fingers of their left hand to mark the Table of Contents and sought the appropriate page with their right hand, which they found cumbersome.

Some participants would like a faster way to flip through pages when scanning or skimming the material. They suggested a PDF-style thumbnail display to give a quick preview. Others would like to be able to view two pages that are not facing pages, which, they said, would help them compare the contents of different parts. This is the reason why only 88% of subjects preferred to read with the page-turning model.

### 7.7 Navigation preferences

There are many possible ways of navigating within the various document formats, and Table 7 shows the functions used by subjects during the user studies. "Scroll bar" means that users move the scroll bar while reading. "Select page" means they position the HTML or PDF scroll bar to a certain location, click on a PDF thumbnail, or select the edge of a page in the book model or physical book. "Hyperlink" means they click a hyperlink in the Table of Contents page, while "bookmark" refers to clicking a bookmark in the PDF bookmark view or a bookmark tab in the book model. The other functions are self-explanatory.

**Table 7** Navigation usage (in %)

Function	HTML	PDF	Book
(a) First user study			
Scroll bar	100	100	N/A
Arrow key	100	100	100
Page Up and Down key	0	0	N/A
Previous and Next button	12	21	17
Type page number	N/A	0	0
Select page	0	0	75
Hyperlink	100	42	100
Bookmark	N/A	100	88
Page turning	N/A	N/A	33
Function	Simulated book	Physical book	
(b) Second user study			
Scroll bar	N/A	N/A	
Arrow key	75	N/A	
Page Up and Down key	N/A	N/A	
Previous and Next button	19	N/A	
Type page number	0	N/A	
Select page	88	100	
Hyperlink	63	N/A	
Bookmark	100	0	
Page turning	12	100	

Most participants using the HTML format did not utilize the browser's *previous* or *next* buttons to return to the Table of Contents; instead they used the scroll bar to go back to the top. While reading a section, they preferred the arrow key rather than the scroll bar, to ensure that they did not miss any text.

Similar behavior can be seen with PDF. While reading, most participants used the *up* and *down* keys to ensure that they read all the information. Because the PDF bookmark view shows the Table of Contents page, few subjects return to this page to find a section. Some did, because they forgot about the bookmark view—they had closed it to enlarge the reading area.

The bookmark view and hyperlink capability available in both PDF and page-turning formats meant that participants did not feel the need to type page numbers—although the page number and total number of pages should still be displayed because they help readers understand where they are in the document. Most users did not click the *next* and *previous* buttons; instead they used the arrow keys to move between consecutive pages.

Users of the book model turned pages with the mouse (rather than the arrow keys) when reading a section of a book, particularly when they were comparing the contents of adjacent pages. Some participants preferred to use page-turning

gestures throughout. All participants—even those who did not use page-turning gestures—remarked that they like the page-turning animation because it made the document more engaging and helped them remember the location of the page. Moreover, they said that if they were reading in their leisure time, they would make more use of page-turning gestures.

## 8 Conclusion

The simple act of turning a page is quite a complicated thing to simulate. This paper has described a variety of models with radically different geometric and physical underpinnings. We have included enough detail to allow readers to understand their basis of operation, and to implement them if desired. We have implemented each algorithm and compared them on the basis of execution speed and visual appearance.

Different degrees of visual accuracy can readily be observed when the simulation results are placed side by side as in Figs. 19 and 20. However, these effects generally go unnoticed when the images are viewed individually, particularly when they are animated under the control of a user who is focused on the page content. For a book using ordinary rectangular flexible pages, the simplest model—two-dimensional peeling as in Fig. 19a—seems adequate for most applications. Although it sacrifices 3D realism, the appearance can be improved by adding visual details to simulate the effect of a smooth bend rather than a sharp crease—some shading on the bend and some shadowing just beneath it—as illustrated in Fig. 2.

The peeling model is inadequate when showing the visual effect of several pages being turned together; the cylindrical and conical models are more suitable for this. If the paper's rigidity and/or shape must be varied, or if users are allowed to make creases—for example, folding corners down into dog-ears—geometric models are inadequate and mass-spring models should be used. In a situation with unlimited computing resources where visual accuracy is more important than interactivity, the finite element method will produce the most realistic simulation for any type of paper under any condition. However, a heavy price is paid in computation time.

In order to investigate how well people interact with realistic page-turning models, we experimented with a lightweight implementation of the peeling method. It provides a quick, easy-to-use, and highly responsive page-turning mechanism, and permits the inclusion of hyperlinks and animated media. This system, which is based on Adobe Flash, is usable within a web browser today. In a user study, readers not only liked the new interface but performed an information finding browsing task significantly quicker than with HTML browser or Adobe Reader, and as quickly as with physical books. User feedback was overwhelmingly positive. Examples can be seen in our book gallery at <http://www.nzdl.org/books>.

**Acknowledgments** We acknowledge with thanks the entire New Zealand Digital Library Project team for their unstinting work in providing an environment that makes this kind of research meaningful—and fun. This study is funded in part by Google.

**Appendix**

This Appendix contains technical details of the finite element method calculations that were omitted from Sect. 5 of the main text. The critical steps concern calculating the strain, obtaining the deformation matrix, and turning the forces into a system of equations that can be integrated to determine the spatial evolution of every finite element at successive time steps.

Calculating the strain

The strain is determined by obtaining the derivatives of the displacement  $\mathbf{d}$  with respect to the  $\xi$ ,  $\eta$  and  $\zeta$  axes and multiplying these by the inverse of the Jacobian matrix.

The Jacobian is defined in Eq. 28, and can be calculated by taking derivatives of point  $\mathbf{p} = (x, y, z)$  from Eq. 23 with respect to the  $\xi$ ,  $\eta$  and  $\zeta$  axes:

$$\begin{aligned} \frac{\partial \mathbf{p}}{\partial \xi} &= \sum_{i=1}^8 \frac{\partial w_i(\xi, \eta)}{\partial \xi} \left( \mathbf{p}_i + \zeta \frac{t_i}{2} \mathbf{n}_i \right) \\ \frac{\partial \mathbf{p}}{\partial \eta} &= \sum_{i=1}^8 \frac{\partial w_i(\xi, \eta)}{\partial \eta} \left( \mathbf{p}_i + \zeta \frac{t_i}{2} \mathbf{n}_i \right) \\ \frac{\partial \mathbf{p}}{\partial \zeta} &= \sum_{i=1}^8 w_i(\xi, \eta) \frac{t_i}{2} \mathbf{n}_i \end{aligned}$$

This yields the value of the Jacobian matrix  $\mathbf{J}$ .

The strain is the derivative of the displacement  $\mathbf{d}$  with respect to the global coordinates  $x, y$  and  $z$ . The displacement is given in terms of the local  $\xi, \eta$  and  $\zeta$  coordinate system by Eq. 25, and its derivatives with respect to those coordinates are:

$$\begin{aligned} \frac{\partial \mathbf{d}}{\partial \xi} &= \sum_{i=1}^8 \frac{\partial w_i(\xi, \eta)}{\partial \xi} \left\{ \begin{bmatrix} u_i \\ v_i \\ w_i \end{bmatrix} + \zeta \frac{t_i}{2} \left( \beta_i \mathbf{e}_i^{\hat{x}} - \alpha_i \mathbf{e}_i^{\hat{y}} \right) \right\} \\ \frac{\partial \mathbf{d}}{\partial \eta} &= \sum_{i=1}^8 \frac{\partial w_i(\xi, \eta)}{\partial \eta} \left\{ \begin{bmatrix} u_i \\ v_i \\ w_i \end{bmatrix} + \zeta \frac{t_i}{2} \left( \beta_i \mathbf{e}_i^{\hat{x}} - \alpha_i \mathbf{e}_i^{\hat{y}} \right) \right\} \\ \frac{\partial \mathbf{d}}{\partial \zeta} &= \sum_{i=1}^8 w_i(\xi, \eta) \frac{t_i}{2} \left( \beta_i \mathbf{e}_i^{\hat{x}} - \alpha_i \mathbf{e}_i^{\hat{y}} \right) \end{aligned}$$

The strain at time  $h$  is obtained by multiplying the above derivatives by  $\mathbf{J}^{-1}$  according to the chain rule, as given in Eq. 27:

$$\begin{aligned} \boldsymbol{\epsilon} &= \begin{bmatrix} \frac{\partial}{\partial x} & 0 & 0 \\ 0 & \frac{\partial}{\partial y} & 0 \\ 0 & 0 & \frac{\partial}{\partial z} \\ \frac{\partial}{\partial y} & \frac{\partial}{\partial x} & 0 \\ \frac{\partial}{\partial z} & 0 & \frac{\partial}{\partial x} \\ 0 & \frac{\partial}{\partial z} & \frac{\partial}{\partial y} \end{bmatrix} \mathbf{d} = \sum_{i=1}^8 \begin{bmatrix} a_i & 0 & 0 \\ 0 & b_i & 0 \\ 0 & 0 & c_i \\ b_i & a_i & 0 \\ c_i & 0 & a_i \\ 0 & c_i & b_i \end{bmatrix} \begin{bmatrix} u_i \\ v_i \\ w_i \end{bmatrix} \\ &+ \begin{bmatrix} f_i & 0 & 0 \\ 0 & g_i & 0 \\ 0 & 0 & h_i \\ g_i & f_i & 0 \\ h_i & 0 & f_i \\ 0 & h_i & g_i \end{bmatrix} \left( \beta_i \mathbf{e}_i^{\hat{x}} - \alpha_i \mathbf{e}_i^{\hat{y}} \right) \\ &= \sum_{i=1}^8 \mathbf{B}_i \mathbf{q}_i \end{aligned}$$

The strain–displacement matrix for  $\mathbf{p}_i$  is

$$\mathbf{B}_i = \begin{bmatrix} a_i & 0 & 0 & -f_i l_i^{\hat{y}} & f_i l_i^{\hat{x}} \\ 0 & b_i & 0 & -g_i m_i^{\hat{y}} & g_i m_i^{\hat{x}} \\ 0 & 0 & c_i & -h_i n_i^{\hat{y}} & h_i n_i^{\hat{x}} \\ b_i & a_i & 0 & -g_i l_i^{\hat{y}} - f_i m_i^{\hat{y}} & g_i l_i^{\hat{x}} + f_i m_i^{\hat{x}} \\ c_i & 0 & a_i & -f_i n_i^{\hat{y}} - h_i l_i^{\hat{y}} & f_i n_i^{\hat{x}} + h_i l_i^{\hat{x}} \\ 0 & c_i & b_i & -h_i m_i^{\hat{y}} - g_i n_i^{\hat{y}} & h_i m_i^{\hat{x}} + g_i n_i^{\hat{x}} \end{bmatrix}$$

where

$$\begin{aligned} a_i &= J_{11}^{-1} \frac{\partial w_i(\xi, \eta)}{\partial \xi} + J_{12}^{-1} \frac{\partial w_i(\xi, \eta)}{\partial \eta} \\ b_i &= J_{21}^{-1} \frac{\partial w_i(\xi, \eta)}{\partial \xi} + J_{22}^{-1} \frac{\partial w_i(\xi, \eta)}{\partial \eta} \\ c_i &= J_{31}^{-1} \frac{\partial w_i(\xi, \eta)}{\partial \xi} + J_{32}^{-1} \frac{\partial w_i(\xi, \eta)}{\partial \eta} \\ f_i &= \frac{t_i}{2} \left( a_i \zeta + J_{13}^{-1} w_i(\xi, \eta) \right) \\ g_i &= \frac{t_i}{2} \left( b_i \zeta + J_{23}^{-1} w_i(\xi, \eta) \right) \\ h_i &= \frac{t_i}{2} \left( c_i \zeta + J_{33}^{-1} w_i(\xi, \eta) \right) \end{aligned}$$

Here,  $J_{ij}^{-1}$  refers to the component of  $\mathbf{J}^{-1}$  at row  $i$ , column  $j$ . The derivatives of the interpolation function  $w_i(\xi, \eta)$  with respect to the  $\xi$  and  $\eta$  axis are given in Table 8.

Calculating the deformation matrix

As explained in Sect. 5.8, the deformation matrix  $\widehat{\mathbf{D}}$  quantifies the relationship between stress and strain at point  $\mathbf{p}$  in the normal-vector coordinate system. The transformation matrix  $\mathbf{Q}$  is used to map  $\widehat{\mathbf{D}}$  to the global coordinate system. The elements of  $\mathbf{Q}$  are obtained from the direction cosines of the  $\hat{x}, \hat{y}, \hat{z}$  coordinate axes at point  $\mathbf{p}$  measured in the  $x, y, z$  coordinate system.

**Table 8** Interpolation function  $w_i(\xi, \eta)$

$i$	$\frac{\partial w_i(\xi, \eta)}{\partial \xi}$	$\frac{\partial w_i(\xi, \eta)}{\partial \eta}$
1	$\frac{1}{4}(2\xi + \eta)(1 - \eta)$	$\frac{1}{4}(1 - \xi)(2\eta + \xi)$
2	$\frac{1}{4}(2\xi - \eta)(1 - \eta)$	$\frac{1}{4}(1 + \xi)(2\eta - \xi)$
3	$\frac{1}{4}(2\xi + \eta)(1 + \eta)$	$\frac{1}{4}(1 + \xi)(2\eta + \xi)$
4	$\frac{1}{4}(2\xi - \eta)(1 + \eta)$	$\frac{1}{4}(1 - \xi)(2\eta - \xi)$
5	$-\xi(1 - \eta)$	$-\frac{1}{2}(1 - \xi^2)$
6	$\frac{1}{2}(1 - \eta^2)$	$-\eta(1 + \xi)$
7	$-\xi(1 + \eta)$	$-\frac{1}{2}(1 - \xi^2)$
8	$\frac{1}{2}(1 - \eta^2)$	$-\eta(1 - \xi)$

The  $\hat{x}$  axis is in a direction perpendicular to the  $\xi$  axis at  $\mathbf{p}$ , namely  $\mathbf{e}^{\hat{x}} = \frac{\mathbf{J}_1}{|\mathbf{J}_1|}$  where the vector  $\mathbf{J}_k$  is the  $k$ th row of the Jacobian matrix. The  $\hat{z}$  axis is in a direction normal to the shell's surface at  $\mathbf{p}$ , and can be obtained by taking the cross product of two different vectors tangential to this surface. It can, therefore, be expressed as  $\mathbf{e}^{\hat{z}} = \frac{\mathbf{J}_1 \times \mathbf{J}_2}{|\mathbf{J}_1 \times \mathbf{J}_2|}$ . Once the directions of the  $\hat{x}$  and  $\hat{z}$  axes are established, the  $\hat{y}$  axis is chosen to be perpendicular to them both; the unit vector along this axis is  $\mathbf{e}^{\hat{y}} = \mathbf{e}^{\hat{x}} \times \mathbf{e}^{\hat{z}}$ .

The components of the matrix  $\mathbf{T}$  are the direction cosines of the normal-vector coordinate system at point  $\mathbf{p}$ , measured in the  $x, y, z$  coordinate system:

$$\mathbf{T} = \begin{bmatrix} \mathbf{e}^{\hat{x}} \\ \mathbf{e}^{\hat{y}} \\ \mathbf{e}^{\hat{z}} \end{bmatrix} = \begin{bmatrix} l^{\hat{x}} & m^{\hat{x}} & n^{\hat{x}} \\ l^{\hat{y}} & m^{\hat{y}} & n^{\hat{y}} \\ l^{\hat{z}} & m^{\hat{z}} & n^{\hat{z}} \end{bmatrix}$$

The matrices  $\widehat{\mathbf{D}}, \mathbf{D}$ , and  $\mathbf{Q}$  are all of the form

$$\begin{bmatrix} A_{1111} & A_{1122} & A_{1133} & A_{1112} & A_{1113} & A_{1123} \\ A_{2211} & A_{2222} & A_{2233} & A_{2212} & A_{2213} & A_{2223} \\ A_{3311} & A_{3322} & A_{3333} & A_{3312} & A_{3313} & A_{3323} \\ A_{1211} & A_{1222} & A_{1233} & A_{1212} & A_{1213} & A_{1223} \\ A_{1311} & A_{1322} & A_{1333} & A_{1312} & A_{1313} & A_{1323} \\ A_{2311} & A_{2322} & A_{2333} & A_{2312} & A_{2313} & A_{2323} \end{bmatrix}$$

The suffixes have a slightly different interpretation in each of the three cases. An element in the local deformation matrix  $\widehat{\mathbf{D}}$  is  $\widehat{D}_{rstu}$ , where  $r, s, t, u \in \{1, 2, 3\}$ . The numbers 1, 2 and 3 signify the  $\hat{x}, \hat{y}$ , and  $\hat{z}$  axes, respectively. The global deformation matrix  $\mathbf{D}$  has elements  $D_{ijkl}$ , with  $i, j, k, l \in \{1, 2, 3\}$ —and here the numbers 1, 2, and 3 signify the  $x, y$ , and  $z$  axes, respectively. The relationship between  $\widehat{\mathbf{D}}$  and  $\mathbf{D}$  is given by the fourth-order tensor transformation

$$D_{ijkl} = \sum_{r=1}^3 \sum_{s=1}^3 \sum_{t=1}^3 \sum_{u=1}^3 T_{ir} T_{js} \widehat{D}_{rstu} T_{kt} T_{lu},$$

where  $T_{ab}$  refers to the component of  $\mathbf{T}$  at row  $a$  and column  $b$ . This transformation can be written in matrix form:

$$\mathbf{D} = \mathbf{Q}^T \widehat{\mathbf{D}} \mathbf{Q}$$

Finally,  $\mathbf{Q}$  is an orthogonal matrix with elements  $Q_{mnop}$ , where  $m, n \in \{1, 2, 3\}$  signify the axes of the global coordinate system and  $o, p \in \{1, 2, 3\}$  the axes of the normal-vector coordinate system:

$$Q_{mnop} = \begin{cases} T_{mo}T_{np} + T_{mp}T_{no} & : o \neq p \\ T_{mo}T_{np} & : o = p \end{cases}$$

Effect of forces

The element's internal energy in Sect. 5.9 is

$$\begin{aligned} \delta E_K + \delta E_P &= \int_V (\delta \mathbf{d})^T (\mathbf{F}_I + \mathbf{F}_D) dV + \int_V (\delta \boldsymbol{\epsilon})^T \boldsymbol{\sigma} dV \\ &= \int_V (\mathbf{w} \delta \mathbf{q})^T (\rho \mathbf{w} \ddot{\mathbf{q}}' + \kappa \mathbf{w} \dot{\mathbf{q}}') dV \\ &\quad + \int_V (\mathbf{B} \delta \mathbf{q})^T (\mathbf{D} \mathbf{B} \mathbf{q}' + \boldsymbol{\sigma}_0) dV \\ &= (\delta \mathbf{q})^T (\mathbf{M} \ddot{\mathbf{q}}' + \mathbf{C} \dot{\mathbf{q}}' + \mathbf{K} \mathbf{q}' + \mathbf{S}_0) \end{aligned}$$

where

$$\mathbf{M} = \int_V \rho \mathbf{w}^T \mathbf{w} dV \tag{35}$$

$$\mathbf{C} = \int_V \kappa \mathbf{w}^T \mathbf{w} dV \tag{36}$$

$$\mathbf{K} = \int_V \mathbf{B}^T \mathbf{D} \mathbf{B} dV \tag{37}$$

$$\mathbf{S}_0 = \int_V \mathbf{B}^T \boldsymbol{\sigma}_0 dV \tag{38}$$

As noted in Eq. 31, conservation of energy implies that this internal energy equates to the element's external energy, which is

$$\begin{aligned} \delta E_T &= \int_V (\delta \mathbf{d})^T \mathbf{F}_B dV + \int_A (\delta \mathbf{d}^A)^T \mathbf{F}_S dA + (\delta \mathbf{q})^T \mathbf{R}_N \\ &= \int_V (\mathbf{w} \delta \mathbf{q})^T \mathbf{F}_B dV + \int_A (\mathbf{w}^A \delta \mathbf{q})^T \mathbf{F}_S dA + (\delta \mathbf{q})^T \mathbf{R}_N \\ &= (\delta \mathbf{q})^T (\mathbf{R}_b + \mathbf{R}_s + \mathbf{R}_N) \end{aligned}$$

where

$$\mathbf{R}_B = \int_V \mathbf{w}^T \mathbf{F}_B dV \tag{39}$$

$$\mathbf{R}_S = \int_A (\mathbf{w}^A)^T \mathbf{F}_S dA \tag{40}$$

Here,  $\mathbf{w}^A$  is obtained from the matrix  $\mathbf{w}$  by substituting the appropriate  $\xi$  and  $\eta$  values.

In order to solve for the values of  $M$ ,  $C$ ,  $K$ ,  $R_B$ ,  $R_S$ , and  $S_0$ , three-point Gaussian quadrature integration is used:

$$\int_V f(V) dV = \int_{-1}^1 \int_{-1}^1 \int_{-1}^1 f(\xi, \eta, \zeta) |\mathbf{J}| d\xi d\eta d\zeta$$

$$\int_A f(A) dA = \int_{-1}^1 \int_{-1}^1 f(\xi, \eta) |\mathbf{J}| d\xi d\eta$$

where  $|\mathbf{J}|$  is the determinant of the Jacobian matrix. In terms of the grid size, the computational complexity of  $f(V)$  and  $f(A)$  is  $O(n^2)$ . The complexity of the finite element method after the integration is  $O(n^4)$ .

## References

1. Bathe, K.J.: Finite Element Procedures. Prentice-Hall, Englewood Cliffs (1995)
2. Beaudouin-Lafon, M.: Novel interaction techniques for overlapping windows. In: UIST '01: Proceedings of the 14th Annual ACM Symposium on User Interface Software and Technology, pp. 153–154 (2001)
3. Bhangal, S.: The page turn effect in flash mx. <http://www.oreillynet.com/pub/a/javascript/2004/09/03/flashhacks.html> (2004)
4. British Library: Turning the pages. <http://www.bl.uk/onlinegallery/ttp/tpbooks.html> (2006)
5. Bucalem, M.L., Bathe, K.J.: Higher-order mitc general shell elements. Int. J. Numer. Methods Eng. **36**, 3729–3754 (1993)
6. Card, S.K., Hong, L., Chen, J.D.: Turning pages of 3D electronic books. In: 2006 IEEE Symposium on 3D User Interfaces, pp. 159–165 (2006)
7. Choi, K.J., Ho, H.S.: Stable but responsive cloth. In: SIGGRAPH 2002 Conference Proceedings: ACM Transactions on Graphics, vol. 21, issue 3, pp. 604–611 (2002)
8. Chu, Y.-C., Witten, I.H., Lobb, R., Bainbridge, D.: How to turn the page. In: JCDL '03: Proceedings of the 3rd ACM/IEEE-CS Joint Conference on Digital Libraries, pp. 186–188 (2003)
9. Chu, Y.-C., Bainbridge, D., Jones, M., Witten, I.H.: Realistic books: a bizarre homage to an obsolete medium? In: JCDL '04: Proceedings of the 4th ACM/IEEE-CS Joint Conference on Digital Libraries, pp. 78–86 (2004)
10. Cushman, W.H.: Reading from microfiche, vdt and the printed page: subjective fatigue and performance. Hum. Factors **28**, 63–73 (1986)
11. Dillon, A., McKnight, C., Richardson, J.: Reading from paper versus reading from screens. Comput. J. **31**, 457–464 (1988)
12. Gotoda, H.: Moving finite elements for simulating creasing phenomena of nearly unstretchable sheet materials. Computer Animation, pp. 21 (2000)
13. Henke, H.: Electronic Books and E-Publishing: A Practical Guide for Authors. Springer Verlag, New York (2001)
14. Kak, A.V.: Relationships between readability of printed and crt-displayed text. In: Proceedings of Human Factors Society Annual Meeting, pp. 137–140 (1981)
15. Liesaputra V., Witten I.H.: Seeking information in realistic books: a user study. In: JCDL '08: Proceedings of the 8th ACM/IEEE-CS Joint Conference on Digital Libraries, pp. 29–38 (2008)
16. Mindlin, R.D.: Influence of rotary inertia and shear on flexural motion of isotropic elastic plates. J. Appl. Mech. **18**, 31–38 (1951)
17. Muter, P., Latremouille, S.A., Treurniet, W.C., Beam, P.: Extended reading of continuous text on television. Hum. Factors **24**, 501–508 (1982)
18. Newmark, N.M.: A method of computation for structural dynamics. ASCE J. Eng. Mech. Div. **85**, 67–94 (1959)
19. O'Shell, S.: Page flip. <http://www.actionscripts.org/showMovie.php?id=459> (2006)
20. Provot, X.: Deformation constraints in a mass-spring model to describe rigid cloth behaviour. In: Proceedings of Graphic Interface '95, pp. 147–154 (1995)
21. Reissner, E.: The effect of transverse shear deformation on the bending of elastic plates. J. Appl. Mech. **67**, A69–A77 (1945)
22. Watt, A.H., Policarpo, F.: The Computer Image. ACM Press, SIGGRAPH Series, Addison-Wesley Longman Ltd (1998)